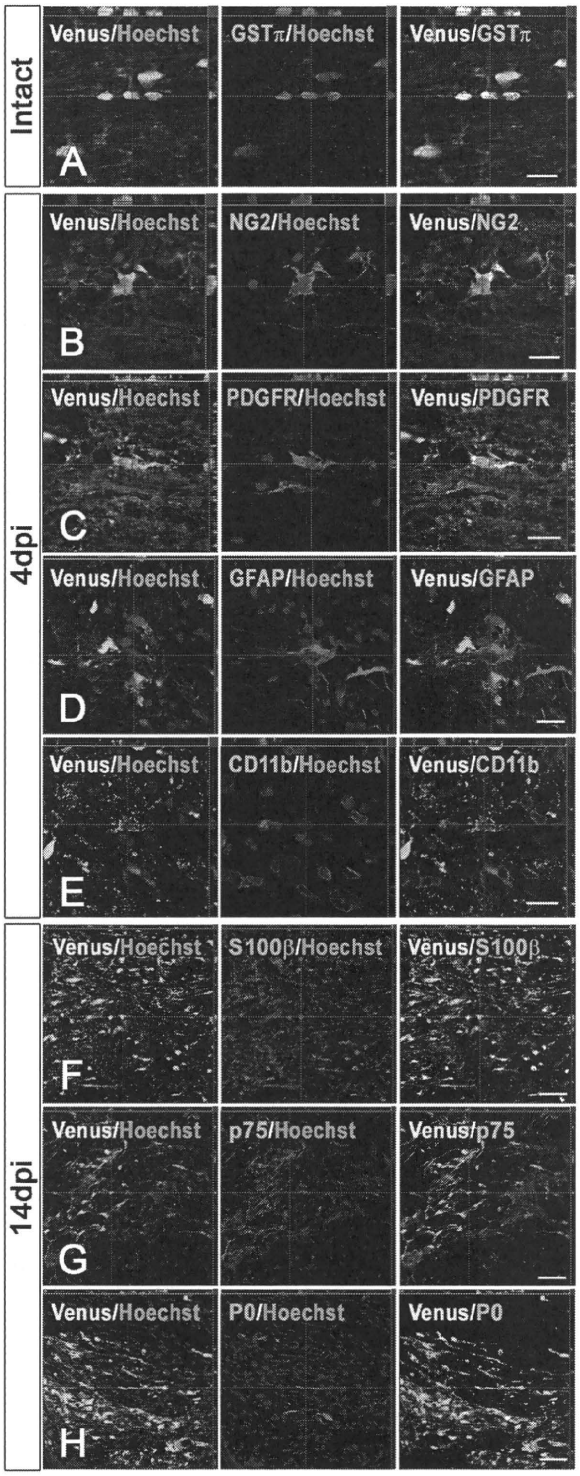

Figure 6 Immunohistochemical analysis of *Sox10*-Venus$^+$ cells after spinal cord injury. (A-E) OPCs and mature oligodendrocytes were Venus$^+$ in the intact and injured spinal cord of *Sox10*-Venus mice. (A) Most Venus$^+$ cells were positive for GSTπ in the intact spinal cord. (B) In the acute phase (4 dpi), NG2$^+$ cells increased in the residual white matter in response to the SCI. Some of the NG2$^+$ cells also expressed Venus. (C-E) In the acute phase, Venus$^+$ oligodendroglial cells were also positive for PDGFRα (C), but were negative for GFAP (D) and CD11b (E). (F) In the subacute phase of the SCI (14 dpi), S100β$^+$ cells were also present around the lesion site, and expressed Venus. (G) Some of the Venus$^+$ cells were positive for p75, suggesting that they were immature Schwann cells with bipolar processes. (H) A small number of Venus$^+$ cells were mature Schwann cells, as assessed by Protein Zero expression. Scale bars; (A-E) 20 μm, (F-H) 50 μm.

Table 1 Comparison of reporter expression in *Sox10*-Venus and various other mice with NC lineage-labeling

Tissues	*Sox10*-Venus	*Sox10*-Cre	*P0*-Cre	*Wnt1*-Cre	*Ht-Pa*-Cre
Dorsal root ganglia	+	+	+	+	+
Sympathetic ganglia	+	+	+	+	+
Melanoblasts	+	+	+	+	+
Enteric nervous system	+	+	+	+	+
Superior/jugular ganglion	+	+	+	+	+
Aortae	+	+	+	+	+
Craniofacial mesenchyme	+	+	+	+	+
Otic vessicle	+	+	+	+	+
Oligodendroglia	+	+	-	-	-
Ventral neural tube	+	+	-	-	-
Developing limb	+	+	-	-	-

Reporter gene expression patterns at the embryonic stage are compared in various mice developed to trace neural crest derivatives: *Sox10*-Venus, *Sox10*(S4F)-Cre [26], *P0*-Cre [5,15], *Wnt1*-Cre [14,16,26,31,32], and *Ht-Pa*-Cre [16,26]. All these lines have similar labeling patterns in both NC-lineage tissues (DRG, sympathetic ganglia, melanoblasts, enteric nervous system, superior/jugular ganglion, aorta, craniofacial mesenchyme) and in tissues not in the NC lineage (otic vesicle, oligodendroglial cells, and OPCs). In the developing limbs of *Sox10*-Venus and *Sox10*-Cre mice, which reflect the endogenous Sox10 expression profile, the reporter fluorescence clearly labeled oligodendroglial cells and the peripheral nervous network. Immunohistochemistry did not detect any ectopic reporter gene expression in any tissues from the embryonic *Sox10*-Venus mice.

The *Sox10*-Venus strain overcomes most of the disadvantages of the above-mentioned *Sox10* reporter mouse lines. In this mouse, the intense Venus fluorescence can be directly observed from outside the embryo, without staining or enhancement procedures (Figure 1, 2, and movies in Additional Files 2 and 3). Venus expression faithfully reflects real-time endogenous Sox10 expression, with prompt on/off switching (Figure 3). Although the choice of strain obviously depends on the purpose of the study, we believe that the *Sox10*-Venus mouse is the most appropriate reporter line for numerous fields of research.

Although *in vivo* time-lapse imaging of oligodendroglial cell migration (including OPCs) has recently been reported, it has only been conducted in zebrafish [33,34]. Accurate time-lapse imaging has been difficult to conduct in mice until now. There are several issues that need to be considered in such studies. For instance, (1) Is the *normal* and *natural* behavior of the cells or tissues of interest being observed? In some cases, the invasive procedures required to complete the imaging, including surgical incision, tissue-slice culture, electroporation, dye injection, and virus infection, may affect the tissues observed. (2) To what degree does the transgenic manipulation affect the phenotype? In $Sox10^{LacZ/+}$ mice, the resulting phenotype, coupled with haploinsufficiency, complicates analysis of the area of interest. Our analysis of the *Sox10*-Venus transgenic line demonstrates that it has neither developmental defects nor ectopic Venus expression. Thus, the *Sox10*-Venus strain appears to be a useful tool for investigating normal developmental processes via live cell monitoring, using directly observed fluorescence without invasive intervention procedures (Figure 1G, movies in Additional Files 2 and 3).

Sox10 is a well-known marker of neural crest stem cells (NCSCs), along with *slug, snail,* and *p75* [35,36]. There have been numerous reports recently of NCSCs surviving in a wide range of tissues through the entire lifespan of the animal, suggesting that NCSCs may have the potential to support the regeneration and recovery of damaged tissues. The Venus fluorescence in *Sox10*-Venus mice will make it possible to prospectively sort $Venus^+$ cells by flow-cytometry and collect an enriched population of NCSCs. Since NCSCs are located in easily accessible peripheral tissues such as the skin and bone marrow, NCSCs have been receiving increasing attention for future clinical applications in cell transplantation therapy, because the feasibility of autologous transplantation is anticipated [37-39]. Autologous cell transplantation therapy avoids the immunological and ethical concerns related to the use of embryonic stem cells. We hope that the *Sox10*-Venus strain will prove to be a powerful tool for enhancing the progress of NCSC research.

The mouse is an excellent model system for studying human disease progression and pathogenesis. We demonstrated the usefulness of our new reporter mouse strain *Sox10*-Venus for monitoring processes occurring after a traumatic disorder (Figure 5 and 6), and crossing it with mutant mouse lines may provide insight into the processes behind numerous developmental defects. As with the analysis conducted in CNP-EGFP mice to study the behavior of oligodendroglial cells in SCI [30], *Sox10*-Venus mice have potential applications not only for oligodendrocyte research, but also for all $Sox10^+$-tissue analyses, including disorders of the NC cells and peripheral nerves. The ability to visualize the processes of disease initiation and progression will help to shed light on the pathophysiology of many human diseases.

Conclusions

We developed the novel *Sox10*-Venus BAC transgenic mouse line, in which Venus fluorescence labels NC and oligodendroglial lineage cells. Endogenous Sox10 expression is accurately reported by Venus fluorescence over the course of normal development, without ectopic Venus expression. The highly intense reporter fluorescence allows for *in vivo* imaging of single-cell migration. This strain will be especially useful for analyzing spinal cord injury and studying NCSCs.

Methods

BAC Construction and development of *Sox10*-venus BAC transgenic mice

For generating the *Sox10*-Venus transgenic mouse, we prepared the following BAC construction. Detailed procedures will be described elsewhere (CA, TI, YUI, manuscript in preparation). Briefly, a BAC clone *RP24-85O14* (CHORI, BACPAC Resources) that covers 225.6 kb territory of mouse *Sox10* gene locus was electroporated into the recombinogenic bacterial strain EL250 for systematic modifications [40]. To obtain in-frame replacement of the exon containing the *Sox10* translation initiation codon (ATG) to the Venus-polyadenylation signal (pA) cassette in the BAC clone, 1.2 kb homology arms were amplified by PCR and sequentially subcloned into the pBluescriptII vector (Stratagene). Then the Venus-pA-FRT-*Kanamycin*-resistant gene (*Kan*^{r})-FRT cassette was inserted in between the arms and the fragment containing the Venus-pA-*Kan*^{r} cassette with the homology arms was isolated by agarose gel electrophoresis for homologous recombination which was processed in EL250 as was reported previously [41]. Precise insertion of the Venus-pA cassette and excision of the *Kan*^{r} in the *Sox10*-BAC was verified by PCR as well as pulse field gel electrophoresis and the modified BAC clone was linearlized by PI-*Sce*I, dialyzed and diluted to ~2 ng/μl for pronuclear injections as previously described [41]. For BAC transgenic mouse founders, presence of *RP24* BAC vector sequences immediately upstream or downstream of the PI-*Sce*I site was always examined by PCR tail DNA analyses to minimize the possibility that fortuitous deletions occur on the BAC transgene after the chromosomal integrations [41]. The established BAC transgenic mouse lines were bred with wild-type C57BL/6J mice and the tail DNA was used for the PCR genotyping: The PCR primers for the transgene detections are provided in Table S1; Additional File 5.

Animals

We purchased wild-type C57BL/6J and ICR mice from SLC Japan. The Cre-expressing transgenic lines, *Wnt1*-Cre [14] and *P0*-Cre [15], were mated with an EGFP reporter line (CAG-CAT-EGFP [18]) to obtain *Wnt1*-Cre/CAG-CAT-EGFP and *P0*-Cre/CAG-CAT-EGFP double-transgenic mice. All mice were housed under specific pathogen-free conditions. All experimental procedures were approved by the Institutional Animal Care and Use Committee of Keio University, Murayama Medical Center, and Tokyo Medical and Dental University. All surgical interventions and animal care procedures were in accordance with the Laboratory Animal Welfare Act, the Guide for the Care and Use of Laboratory Animals (National Institute of Health, USA).

Histological analysis

Immunohistochemical analyses were performed as described previously [5,42,43]. Briefly, E9.5 d, n = 3; E10.5 d, n = 10; E11.5 d, n = 9; E12.5 d, n = 5; E13.5 d, n = 6; E14.5 d, n = 3; E15.5 d, n = 7; E16.5 d, n = 3; P0 d, n = 3; and P1 w, n = 3 transgenic embryos (E0 = day of plug) and pups were fixed with 4% PFA, and 16-μm-thick cryosections were prepared with the cryostat CM3000 (Leica). The detailed information about the primary and secondary antibodies was described in Table S1; Additional File 5. Antigen retrieval was applied for specific targets (anti-Olig2, anti-hSox10) by incubating them with Target Retrieval Solution (Dako) in an autoclave at 105°C for 5 minutes. Fluorescence immunostaining with specific primary antibodies was performed overnight at 4° C, followed by one-hour incubation at room temperature with the appropriate secondary antibodies conjugated with Alexa488, Alexa555, or Alexa647 (Invitrogen) along with Hoechst 33258 (10 μg/ml, Sigma) for nuclear staining. The samples were examined with a laser scanning confocal microscope (LSM700 or Pascal: Carl Zeiss) or fluorescent microscope (BZ-9000: Keyence, MVX-CSU: Olympus).

Time-Lapse Imaging

Time-lapse observation (Figure 1G, movies in Additional Files 2 and 3) was performed as described previously [44,45]. Briefly, freshly isolated embryos were collected in cold phosphate buffered saline (PBS) and genotyped based on their Venus fluorescence, using an inverted epifluorecence microscope (Leica MZ10F). The embryos were transferred with 100 - 150 μl of enriched medium to the center of a 35-mm glass-bottom dish (hole size 27 mm; Matsunami) and mixed with 100-150 μl of type I collagen-gel solution (Cellmatrix IA; Nitta Gelatin). The solution had been previously diluted to 0.5-0.6 mg/ml with distilled water, 5× DMEM, and a neutralizing buffer, with a final concentration about 0.3 mg/ml, according to the manufacturer's protocol. The gel was incubated at 37° C for 20 minutes. Once the gel was solidified, up to 600 μl of imaging culture medium was gently added to

the gel. The final concentration of the culture medium was as follows: DMEM/F-12 (1:1), glucose (0.6%), L-glutamine (2 mM), sodium bicarbonate (3 mM), HEPES buffer (50 mM), insulin (25 μg/ml), transferrin (100 μg/ml), progesterone (20 nM), sodium selenate (30 nM), and putrescine (60 μM), with equilibration buffer supplemented with 4% fetal bovine serum. The dish was attached to a pre-heated microscope stage and incubated at 37°C in 5% CO_2. Imaging was carried out with an epifluorescence microscope from Keyence (BZ9000) or a confocal Carl Zeiss microscope (LSM5 PASCAL Exciter). Images were acquired with a 10× objective lens every 10 or 20 minutes, and processed using the Keyence Bz-II application and Zeiss LSM5 software, respectively. NIH ImageJ 1.44e and Quicktime Pro 7.6.8 were used for preparing movie files.

Spinal cord injury model

Adult female *Sox10*-Venus mice (8-weeks old, n = 4 for each time point) were anesthetized with an intraperitoneal injection of ketamine (100 mg/kg) and xylazine (10 mg/kg). The dorsal surface of the dura mater was exposed after laminectomy at the tenth thoracic vertebra, and SCI was induced using an IH (Infinite Horizon) impactor (60 kDyn; Precision Systems & Instrumentation) as described previously [46,47]. The mice were returned to their home cages with free access to water and food. Intact mice and mice at 4 and 14 days post-injury (dpi) were deeply anesthetized and transcardially perfused with chilled PBS followed by 4% paraformaldehyde (PFA). The spinal cords were removed and immersed in 4% PFA at 4°C overnight, and then immersed in 15% and 30% sucrose for 24 hours each, at 4°C. The spinal cords were then embedded in OCT compound and sectioned into 12-μm-thick sagittal sections by cryostat (Leica CM3000).

Additional material

Additional file 1: Embryonic age-dependent fluorescence changes compared among the *Sox10*-Venus, P0-Cre/CAG-CAT-EGFP, and *Wnt1*-Cre/CAG-CAT-EGFP mouse strain. (A-C) Venus fluorescence changes over time were observed from outside of the *Sox10*-Venus embryo. Deep-tissue fluorescence gradually decreased from E11.5 d to E15.5 d (see Figure 1 for additional photos). (C-E) At E14.5 d, reporter gene expression patterns were quite similar between the transgenic *Sox10*-Venus mouse and the double-transgenic mice *P0*-Cre/CAG-CAT-EGFP and *Wnt1*-Cre/CAG-CAT-EGFP. Scale bars (A-E) 1.0 mm.

Additional file 2: Live imaging of single-cell movement: *Sox10*-Venus$^+$ NC-derivatives in the superficial embryonic skin layer (1). Time-lapse imaging with an epifluorescence microscope (Keyence) showed Venus-positive cell movements in E14.5 d *Sox10*-Venus embryo ex-vivo skin explants. One frame was captured every 10 minutes over a 6-hour period (motion: 6 fps).

Additional file 3: Live imaging of single-cell movement: *Sox10*-Venus$^+$ neural crest derivatives in the superficial embryonic skin layer (2). Confocal time-lapse imaging of the front facial area of the whole E10.5 d *Sox10*-Venus embryo captured isolated Venus-positive cells. The distinctive, intense Venus fluorescence made it possible to follow migrating cells within the embryo over several hours, even capturing the dynamic changes in cell shape. One frame was captured every 20 minutes using a confocal Pascal microscope (Carl Zeiss). Scale bar: 50 μm, motion: 4 fps.

Additional file 4: NC progeny were permanently EGFP-labeled in the *Wnt1*-Cre/CAG-CAT-EGFP mouse. (A-B) Immunohistochemical analysis with anti-GFP and marker antibodies for specific cell types showed that the EGFP reporter gene is continuously expressed in NC derivatives in the DRG (A) and sympathetic ganglia (B) of E15.5 d *Wnt1*-Cre/CAG-CAT-EGFP mice. Scale bars (A-B) 50 μm.

Additional file 5: Table S1: Detailed information about sequences and antibodies.

Abbreviations

NC: neural crest; OPC: oligodendrocyte progenitor cell; HMG: high mobility group; PNS: peripheral nervous system; CNS: central nervous system; P0: protein zero; EGFP: enhanced green fluorescent protein; CNP: 2'-3'-cyclic nucleotide 3'-phosphodiesterase; PLP: myelin proteolipid protein; TH: tyrosine hydroxylase; DRG: dorsal root ganglia; SCI: spinal cord injury; DPI: days-post-injury; p75: p75 neurotrophin receptor; NSPC: neural stem/progenitor cell; NCSCs: neural crest stem cells; PBS: phosphate buffered saline.

Acknowledgements

We are grateful to Dr. R.B. Darnell for the gift of the anti-Hu antibody. We are grateful to Drs. C. Hara, N. Kishi, N. Shimojima, M. Mori, A. Iwanami, and H. Kanki for their excellent technical instruction and for critical reading of the manuscript. We also thank all the members in the Okano Laboratory and Akazawa Laboratory for their encouragement and invaluable comments on this manuscript.

This work was supported by a Grant-in-Aid for Young Scientists and a Grant-in-Aid for Scientific Research (C) from The Ministry of Education, Culture, Sports, Science and Technology, Japan (MEXT) to S.S. and F.R-M.; by a Keio University Grant-in-Aid for the Encouragement of Young Medical Scientists to S.S. and F.R-M.; by Keio Gijuku Academic Development Funds to S.S.; by a JST-SORST fellowship to F.R-M.; by grants from Research Foundation ITSUU Laboratory and Takeda Science Foundation to T. I.; and by a Grant-in-Aid from the Global COE Program of the MEXT to Keio University to H.O.

Author details

[1]Department of Physiology, Keio University School of Medicine, Shinjuku-ku, Tokyo 160-8582, Japan. [2]Department of Orthopaedic Surgery, Keio University School of Medicine, Shinjuku-ku, Tokyo 160-8582, Japan. [3]Clinical Research Center, National Hospital Organization, Murayama Medical Center, 2-37-1 Gakuen, Musashimurayama, Tokyo 208-0011, Japan. [4]Department of Biochemistry and Cellular Biology, National Institute of Neuroscience, NCNP, Tokyo 187-8502, Japan. [5]Department of Biochemistry and Biophysics, Graduate School of Health and Sciences, Tokyo Medical and Dental University, Bunkyo, Tokyo, Japan.

Authors' contributions

SS, CA, and HO designed the project. SS, AY, FRM, SS, TI, YUI, NN, and MS performed experiments and analyzed the data. SS, AY, and FRM prepared the figures. SS, AY, FRM, HK, TI, MN, CA, and HO wrote the manuscript. MN, CA, and HO supervised the project. All authors read and approved the final manuscript.

Competing interests

The authors declare that they have no competing interests.

Received: 23 October 2010 Accepted: 31 October 2010
Published: 31 October 2010

References

1. Le Douarin NM, Kalcheim C: *The Neural Crest*. 2 edition. New York, NY: Cambridge University Press; 1999.

2. Le Douarin NM, Creuzet S, Couly G, Dupin E: **Neural crest cell plasticity and its limits.** *Development* 2004, **131**:4637-4650.
3. Le Douarin NM, Dupin E: **Multipotentiality of the neural crest.** *Curr Opin Genet Dev* 2003, **13**:529-536.
4. Morikawa S, Mabuchi Y, Niibe K, Suzuki S, Nagoshi N, Sunabori T, Shimmura S, Nagai Y, Nakagawa T, Okano H, Matsuzaki Y: **Development of mesenchymal stem cells partially originate from the neural crest.** *Biochem Biophys Res Commun* 2009, **379**:1114-1119.
5. Nagoshi N, Shibata S, Kubota Y, Nakamura M, Nagai Y, Satoh E, Morikawa S, Okada Y, Mabuchi Y, Katoh H, *et al*: **Ontogeny and multipotency of neural crest-derived stem cells in mouse bone marrow, dorsal root ganglia, and whisker pad.** *Cell Stem Cell* 2008, **2**:392-403.
6. Bowles J, Schepers G, Koopman P: **Phylogeny of the SOX family of developmental transcription factors based on sequence and structural indicators.** *Dev Biol* 2000, **227**:239-255.
7. Wegner M: **From head to toes: the multiple facets of Sox proteins.** *Nucleic Acids Res* 1999, **27**:1409-1420.
8. Haldin CE, LaBonne C: **SoxE factors as multifunctional neural crest regulatory factors.** *Int J Biochem Cell Biol* 2010, **42**:441-444.
9. Kuhlbrodt K, Schmidt C, Sock E, Pingault V, Bondurand N, Goossens M, Wegner M: **Functional analysis of Sox10 mutations found in human Waardenburg-Hirschsprung patients.** *J Biol Chem* 1998, **273**:23033-23038.
10. Southard-Smith EM, Kos L, Pavan WJ: **Sox10 mutation disrupts neural crest development in Dom Hirschsprung mouse model.** *Nat Genet* 1998, **18**:60-64.
11. Inoue K, Khajavi M, Ohyama T, Hirabayashi S, Wilson J, Reggin JD, Mancias P, Butler IJ, Wilkinson MF, Wegner M, Lupski JR: **Molecular mechanism for distinct neurological phenotypes conveyed by allelic truncating mutations.** *Nat Genet* 2004, **36**:361-369.
12. Inoue K, Tanabe Y, Lupski JR: **Myelin deficiencies in both the central and the peripheral nervous systems associated with a SOX10 mutation.** *Ann Neurol* 1999, **46**:313-318.
13. Pingault V, Bondurand N, Kuhlbrodt K, Goerich DE, Prehu MO, Puliti A, Herbarth B, Hermans-Borgmeyer I, Legius E, Matthijs G, *et al*: **SOX10 mutations in patients with Waardenburg-Hirschsprung disease.** *Nat Genet* 1998, **18**:171-173.
14. Danielian PS, Muccino D, Rowitch DH, Michael SK, McMahon AP: **Modification of gene activity in mouse embryos in utero by a tamoxifen-inducible form of Cre recombinase.** *Curr Biol* 1998, **8**:1323-1326.
15. Yamauchi Y, Abe K, Mantani A, Hitoshi Y, Suzuki M, Osuzu F, Kuratani S, Yamamura K: **A novel transgenic technique that allows specific marking of the neural crest cell lineage in mice.** *Dev Biol* 1999, **212**:191-203.
16. Pietri T, Eder O, Blanche M, Thiery JP, Dufour S: **The human tissue plasminogen activator-Cre mouse: a new tool for targeting specifically neural crest cells and their derivatives in vivo.** *Dev Biol* 2003, **259**:176-187.
17. Soriano P: **Generalized lacZ expression with the ROSA26 Cre reporter strain.** *Nat Genet* 1999, **21**:70-71.
18. Kawamoto S, Niwa H, Tashiro F, Sano S, Kondoh G, Takeda J, Tabayashi K, Miyazaki J: **A novel reporter mouse strain that expresses enhanced green fluorescent protein upon Cre-mediated recombination.** *FEBS Lett* 2000, **470**:263-268.
19. Yoshida S, Shimmura S, Nagoshi N, Fukuda K, Matsuzaki Y, Okano H, Tsubota K: **Isolation of multipotent neural crest-derived stem cells from the adult mouse cornea.** *Stem Cells* 2006, **24**:2714-2722.
20. Tomita Y, Matsumura K, Wakamatsu Y, Matsuzaki Y, Shibuya I, Kawaguchi H, Ieda M, Kanakubo S, Shimazaki T, Ogawa S, *et al*: **Cardiac neural crest cells contribute to the dormant multipotent stem cell in the mammalian heart.** *J Cell Biol* 2005, **170**:1135-1146.
21. Aihara Y, Hayashi Y, Hirata M, Ariki N, Shibata S, Nagoshi N, Nakanishi M, Ohnuma K, Warashina M, Michiue T, *et al*: **Induction of neural crest cells from mouse embryonic stem cells in a serum-free monolayer culture.** *Int J Dev Biol* 2010, **54**:1287-1294.
22. Mallon BS, Shick HE, Kidd GJ, Macklin WB: **Proteolipid promoter activity distinguishes two populations of NG2-positive cells throughout neonatal cortical development.** *J Neurosci* 2002, **22**:876-885.
23. Yuan X, Chittajallu R, Belachew S, Anderson S, McBain CJ, Gallo V: **Expression of the green fluorescent protein in the oligodendrocyte lineage: A transgenic mouse for developmental and physiological studies.** *Journal of Neuroscience Research* 2002, **70**:529-545.
24. Britsch S, Goerich DE, Riethmacher D, Peirano RI, Rossner M, Nave KA, Birchmeier C, Wegner M: **The transcription factor Sox10 is a key regulator of peripheral glial development.** *Genes Dev* 2001, **15**:66-78.
25. Ludwig A, Schlierf B, Schardt A, Nave KA, Wegner M: **Sox10-rtTA mouse line for tetracycline-inducible expression of transgenes in neural crest cells and oligodendrocytes.** *genesis* 2004, **40**:171-175.
26. Stine ZE, Huynh JL, Loftus SK, Gorkin DU, Salmasi AH, Novak T, Purves T, Miller RA, Antonellis A, Gearhart JP, *et al*: **Oligodendroglial and pan-neural crest expression of Cre recombinase directed bySox10enhancer.** *genesis* 2009, **47**:765-770.
27. Nagai T, Ibata K, Park ES, Kubota M, Mikoshiba K, Miyawaki A: **A variant of yellow fluorescent protein with fast and efficient maturation for cell-biological applications.** *Nat Biotechnol* 2002, **20**:87-90.
28. Breuskin I, Bodson M, Thelen N, Thiry M, Borgs L, Nguyen L, Lefebvre PP, Malgrange B: **Sox10 promotes the survival of cochlear progenitors during the establishment of the organ of Corti.** *Developmental Biology* 2009, **335**:327-339.
29. Breuskin I, Bodson M, Thelen N, Thiry M, Borgs L, Nguyen L, Stolt C, Wegner M, Lefebvre PP, Malgrange B: **Glial but not neuronal development in the cochleo-vestibular ganglion requires Sox10.** *J Neurochem* 2010, **114**:1827-1839.
30. Lytle JM, Chittajallu R, Wrathall JR, Gallo V: **NG2 cell response in the CNP-EGFP mouse after contusive spinal cord injury.** *Glia* 2009, **57**:270-285.
31. Brault V, Moore R, Kutsch S, Ishibashi M, Rowitch DH, McMahon AP, Sommer L, Boussadia O, Kemler R: **Inactivation of the beta-catenin gene by Wnt1-Cre-mediated deletion results in dramatic brain malformation and failure of craniofacial development.** *Development* 2001, **128**:1253-1264.
32. Chai Y, Jiang X, Ito Y, Bringas P Jr, Han J, Rowitch DH, Soriano P, McMahon AP, Sucov HM: **Fate of the mammalian cranial neural crest during tooth and mandibular morphogenesis.** *Development* 2000, **127**:1671-1679.
33. Kirby BB, Takada N, Latimer AJ, Shin J, Carney TJ, Kelsh RN, Appel B: **In vivo time-lapse imaging shows dynamic oligodendrocyte progenitor behavior during zebrafish development.** *Nature Neuroscience* 2006, **9**:1506-1511.
34. Takada N, Kucenas S, Appel B: **Sox10 is necessary for oligodendrocyte survival following axon wrapping.** *Glia* 2010, **58**:996-1006.
35. Crane JF, Trainor PA: **Neural crest stem and progenitor cells.** *Annu Rev Cell Dev Biol* 2006, **22**:267-286.
36. Delfino-Machin M, Chipperfield TR, Rodrigues FS, Kelsh RN: **The proliferating field of neural crest stem cells.** *Dev Dyn* 2007, **236**:3242-3254.
37. Aki R, Amoh Y, Li L, Katsuoka K, Hoffman RM: **Nestin-expressing interfollicular blood vessel network contributes to skin transplant survival and wound healing.** *J Cell Biochem* 2010, **110**:80-86.
38. Jinno H, Morozova O, Jones KL, Biernaskie JA, Paris M, Hosokawa R, Rudnicki MA, Chai Y, Rossi F, Marra MA, Miller FD: **Convergent Genesis of an Adult Neural Crest-Like Dermal Stem Cell From Distinct Developmental Origins.** *Stem Cells* 2010.
39. Amoh Y, Li L, Katsuoka K, Hoffman RM: **Multipotent hair follicle stem cells promote repair of spinal cord injury and recovery of walking function.** *Cell Cycle* 2008, **7**:1865-1869.
40. Lee EC, Yu D, Martinez de Velasco J, Tessarollo L, Swing DA, Court DL, Jenkins NA, Copeland NG: **A highly efficient Escherichia coli-based chromosome engineering system adapted for recombinogenic targeting and subcloning of BAC DNA.** *Genomics* 2001, **73**:56-65.
41. Inoue T, Inoue YU, Asami J, Izumi H, Nakamura S, Krumlauf R: **Analysis of mouse Cdh6 gene regulation by transgenesis of modified bacterial artificial chromosomes.** *Dev Biol* 2008, **315**:506-520.
42. Sakakibara S, Nakamura Y, Satoh H, Okano H: **Rna-binding protein Musashi2: developmentally regulated expression in neural precursor cells and subpopulations of neurons in mammalian CNS.** *J Neurosci* 2001, **21**:8091-8107.
43. Sakakibara S, Nakamura Y, Yoshida T, Shibata S, Koike M, Takano H, Ueda S, Uchiyama Y, Noda T, Okano H: **RNA-binding protein Musashi family: roles for CNS stem cells and a subpopulation of ependymal cells revealed by targeted disruption and antisense ablation.** *Proc Natl Acad Sci USA* 2002, **99**:15194-15199.

44. Miyata T, Nakajima K, Mikoshiba K, Ogawa M: **Regulation of Purkinje cell alignment by reelin as revealed with CR-50 antibody.** *J Neurosci* 1997, **17**:3599-3609.
45. Miyata T, Ogawa M: **Twisting of neocortical progenitor cells underlies a spring-like mechanism for daughter-cell migration.** *Curr Biol* 2007, **17**:146-151.
46. Kumagai G, Okada Y, Yamane J, Nagoshi N, Kitamura K, Mukaino M, Tsuji O, Fujiyoshi K, Katoh H, Okada S, *et al*: **Roles of ES cell-derived gliogenic neural stem/progenitor cells in functional recovery after spinal cord injury.** *PLoS One* 2009, **4**:e7706.
47. Scheff SW, Rabchevsky AG, Fugaccia I, Main JA, Lumpp JE Jr: **Experimental modeling of spinal cord injury: characterization of a force-defined injury device.** *J Neurotrauma* 2003, **20**:179-193.

doi:10.1186/1756-6606-3-31
Cite this article as: Shibata *et al.*: *Sox10*-Venus mice: a new tool for real-time labeling of neural crest lineage cells and oligodendrocytes. *Molecular Brain* 2010 **3**:31.

Experimental Neurology 224 (2010) 403–414

Contents lists available at ScienceDirect

Experimental Neurology

journal homepage: www.elsevier.com/locate/yexnr

Anti-IL-6-receptor antibody promotes repair of spinal cord injury by inducing microglia-dominant inflammation

Masahiko Mukaino [a,b], Masaya Nakamura [c,*], Osamu Yamada [b], Seiji Okada [d], Satoru Morikawa [e], Francois Renault-Mihara [b], Akio Iwanami [c,f], Takeshi Ikegami [c,f], Yoshiyuki Ohsugi [g], Osahiko Tsuji [c], Hiroyuki Katoh [f], Yumi Matsuzaki [b], Yoshiaki Toyama [c], Meigen Liu [a], Hideyuki Okano [b,*]

[a] Department of Rehabilitation Medicine, Keio University School of Medicine, Shinjuku, Tokyo 160-8582, Japan
[b] Department of Physiology, Keio University School of Medicine, Shinjuku, Tokyo 160-8582, Japan
[c] Department of Orthopedic Surgery, Keio University School of Medicine, Shinjuku, Tokyo 160-8582, Japan
[d] Department of Research Superstar Program Stem Cell Unit, Graduate School of Medical Science, Kyushu University, Fukuoka 812-8582, Japan
[e] Department of Dentistry and Oral Surgery, Keio University School of Medicine, Shinjuku, Tokyo 160-8582, Japan
[f] National Hospital Organization, Murayama Medical Center, Musashimurayama, Tokyo 208-0011, Japan
[g] Chugai Pharmaceutical Co. Ltd., Chuo, Tokyo 103-8324, Japan

ARTICLE INFO

Article history:
Received 16 October 2009
Revised 29 April 2010
Accepted 30 April 2010
Available online 16 May 2010

Keywords:
Spinal cord injury
Interleukin-6
Antibody
Inflammation
Microglia
Hematogenous macrophages

ABSTRACT

We previously reported the beneficial effect of administering an anti-mouse IL-6 receptor antibody (MR16-1) immediately after spinal cord injury (SCI). The purpose of our present study was to clarify the mechanism underlying how MR16-1 improves motor function after SCI. Quantitative analyses of inflammatory cells using flow cytometry, and immunohistochemistry with bone marrow-chimeric mice generated by transplanting genetically marked purified hematopoietic stem cells, revealed that MR16-1 dramatically switched the central player in the post-traumatic inflammation, from hematogenous macrophages to resident microglia. This change was accompanied by alterations in the expression of relevant cytokines within the injured spinal cord; the expression of recruiting chemokines including CCL2, CCL5, and CXCL10 was decreased, while that of Granulocyte/Macrophage-Colony Stimulating Factor (GM-CSF), a known mitogen for microglia, was increased. We also showed that the resident microglia expressed higher levels of phagocytic markers than the hematogenous macrophages. Consistent with these findings, we observed significantly decreased tissue damage and reduced levels of myelin debris and Nogo-A, the axonal growth inhibitor, by MR16-1 treatment. Moreover, we observed increased axonal regeneration and/or sprouting in the MR16-1-treated mice. Our findings indicate that the functional improvement elicited by MR16-1 involves microglial functions, and provide new insights into the role of IL-6 signaling in the pathology of SCI.

Introduction

In the pathology of spinal cord injury (SCI), the primary mechanical injury is followed by post-traumatic inflammation, in which inflammatory cells such as neutrophils, hematogenous macrophages (blood-borne macrophages), and resident microglia accumulate at the lesion site. These inflammatory cells release reactive oxygen, nitrogen radicals, and proteases, which exacerbate tissue damage (Hausmann, 2003). Because the inflammation is regulated by pro-inflammatory cytokines, such as TNFα, IL-1β, and IL-6, these cytokines have been targets for potential pharmaceutical interventions for SCI (Nesic et al., 2001; Okada et al., 2004; Sharma et al., 2003; Tuna et al., 2001). Among these cytokines, IL-6 is known to promote the activation and infiltration of macrophages/microglia (Hurst et al., 2001; Van Wagoner and Benveniste, 1999), which are the major inflammatory cells in the injured spinal cord, and the overexpression of IL-6 extends the inflammation to worsen the tissue injury (Klusman and Schwab, 1997; Lacroix et al., 2002). Hypothesizing that a blockade of IL-6 signaling might reduce the extension of injury by post-SCI inflammation, we previously administered the anti-mouse IL6-receptor antibody (MR16-1) after SCI and demonstrated reduced inflammation, decreased astrogliosis, and enhanced tissue sparing, leading to improved functional recovery (Okada et al., 2004). As a humanized antibody for the human IL-6 receptor (MRA; tocilizumab) is already in clinical use for the treatment of Castleman's disease and rheumatoid arthritis (Choy et al., 2002; Nishimoto et al., 2000; Sato et al., 1993), this drug might represent a new option for the treatment of SCI.

* Corresponding authors. H. Okano is to be contacted at the Department of Physiology, Keio University School of Medicine, 35 Shinanomachi, Shinjuku, Tokyo 160-8582, Japan. M. Nakamura, Department of Orthopedic Surgery, Keio University School of Medicine, Shinjuku, Tokyo 160-8582, Japan. Fax: +81 3 3357 5445.
E-mail addresses: masa@sc.itc.keio.ac.jp (M. Nakamura), hidokano@sc.itc.keio.ac.jp (H. Okano).

0014-4886/$ – see front matter © 2010 Elsevier Inc. All rights reserved.
doi:10.1016/j.expneurol.2010.04.020

However, recent studies using gene-knockout animals revealed that the continuous inhibition of IL-6 signaling is detrimental to functional recovery, by inhibiting axonal regeneration or causing failed gliosis, implying that IL-6 may also have a beneficial function in spinal cord repair (Cafferty et al., 2004; Okada et al., 2006). Furthermore, numerous studies suggest that inflammation is beneficial or even essential for spinal cord repair, because it clears tissue debris and involves the secretion of various neurotrophic factors (Donnelly and Popovich, 2008; Hashimoto et al., 2005; McTigue et al., 2000). This discrepancy prompted us to investigate how the administration of an anti-IL-6 receptor antibody immediately after SCI promotes the repair process.

One of the important determinants of the extent of secondary damage by inflammation is the nature of the recruited inflammatory cells. For example, the transplantation of macrophages that have been co-incubated with peripheral nerves or skin improves spinal cord repair (Bomstein et al., 2003; Schwartz et al., 1999). On the other hand, zymosan-activated macrophages have neurotoxic properties, although they can also have proregenerative effects (Gensel et al., 2009; Popovich et al., 2002; Steinmetz et al., 2005). Previous reports have shown that these differences in the characteristics of inflammatory cells depend not only on their state of activation, but also on their origin. A subpopulation of hematogenous macrophages is more cytotoxic than microglia, and their excessive infiltration into a lesion is detrimental to spinal cord repair (Gris et al., 2004; Popovich et al., 1999). Since IL-6 is known to promote macrophage infiltration after central nervous system (CNS) trauma (Klusman and Schwab, 1997; Lacroix et al., 2002), here we focused on the effect of the temporary inhibition of IL-6 signaling by MR16-1 on macrophages and microglia after SCI. The administration of MR16-1 reduced the infiltration of macrophages into the injured spinal cord, but increased the number of microglia residing there, thus switching the major inflammatory cell type at the lesion from hematogenous macrophages to resident microglia. A comparison of the expression of phagocytic markers by hematogenous macrophages and microglia revealed that the microglia had greater phagocytic ability against myelin debris after SCI. Consequently, this switch in major inflammatory cell type resulted in improved tissue sparing and debris clearance, which promoted neural repair after SCI.

Materials and methods

Animals

74 adult female C57BL/6J mice (8–10 weeks old) were used. C57BL/6 background CAG-EGFP transgenic mice that ubiquitously express EGFP under the control of the CAG promoter (Kawamoto et al., 2000) were kindly provided by Professor Jun-ichi Miyazaki (Osaka University, Osaka, Japan) and were bred in our animal facility. The ethics committee of our institution approved all the surgical and animal care procedures, in accordance with the Laboratory Animal Welfare Act, the Guide for the Care and Use of Laboratory Animals (National Institutes of Health), and the Guidelines and Policies for Animal Surgery provided by the Animal Study Committees of the Central Institute for Experimental Animals and of Keio University.

Rat anti-mouse IL-6 receptor monoclonal antibody (MR16-1)

The rat anti-mouse IL-6 receptor monoclonal antibody MR16-1 was prepared as described previously (Tamura et al., 1993). MR16-1 binds to the mouse IL-6 receptor and suppresses IL-6-induced cellular responses in a dose-dependent manner (Okazaki et al., 2002). Other basic characterizations of this antibody were reported previously (Okazaki et al., 2002; Tamura et al., 1993).

Purification and transplantation of genetically marked hematopoietic stem cells (HSCs)

In the present study, we produced bone marrow-chimeric mice using highly purified, genetically marked hematopoietic stem cells by the method reported by Koide et al. (2007). This method enabled us to limit our observation specifically to the hematopoietic cell lineage. The femurs and tibias were dissected from donor CAG-EGFP transgenic mice and crushed with a pestle. The marrow cells were collected in HBSS+ (Hanks-balanced salt solution supplemented with 2% FCS, 10 mM HEPES, and 1% penicillin/streptomycin), filtered through a cell strainer (Falcon 2350) to remove debris, and suspended in 50 ml of ice-cold HBSS+. The cells were collected by centrifugation at 280 g for 6 min at 4 °C, resuspended in HBSS+ at 1×10^6 cells/ml, and incubated with 5 μg/ml Hoechst 33342 (Sigma Chemical Co.) for 60 min at 37 °C. A parallel aliquot was stained with Hoechst dye in the presence of 50 μM reserpine (Sigma Chemical Co.). The cells were spun down, resuspended in 5 ml of ice-cold HBSS+, and layered on top of 5 ml of Ficoll-Paque™ Plus (Amersham Pharmacia Biotech AB, Uppsala, Sweden). After centrifugation at 630 g at 4 °C for 20 min, the mononuclear cells were collected from the intermediate layer and immediately washed with 10 ml of ice-cold HBSS+. The Hoechst-stained cells were resuspended in ice-cold HBSS+ at $1\text{–}5\times10^7$ cells/ml and stained for 30 min on ice with one of the following monoclonal antibodies: biotinylated CD34 (RAM34), PE-conjugated Sca-1 (Ly6A/E), or APC-conjugated c-Kit (2B8). Biotinylated antibodies were visualized with Cy7-APC-conjugated streptavidin. All of these reagents were purchased from eBioscience (San Diego, CA). An aliquot of cells was also stained with a mouse isotype control conjugated with FITC, PE, or APC. After antibody staining, the cells were washed in an excess volume of HBSS+ and resuspended at 1×10^7 cells/ml in HBSS+ containing 2 μg/ml propidium iodide (PI; Sigma Chemical Co.). Genetically marked, highly purified HSCs ($CD34^-$ $Sca\text{-}1^+$ $c\text{-}kit^+$ SP cells (Matsuzaki et al., 2004)) derived from donor CAG-EGFP transgenic animals were sorted by flow cytometry. A 100-μl aliquot of unfractionated marrow cell suspension (2×10^5 cells) from donors not carrying the CAG-EGFP transgene was added to provide competitor cells, which is the minimum dose to keep the animals alive during the period required for bone marrow reconstitution. A suspension of 100 $CD34^-$ $Csa\text{-}1^+$ $c\text{-}kit^+$ SP cells and 2×10^5 unfractionated marrow cells was then intravenously injected into the retro-orbital plexus of an etherized recipient mouse that had been lethally irradiated at 10.5 Gy. The successful induction of chimerism was confirmed by a Dual-laser FACS Calibur (Becton and Dickinson, CA) analysis of the peripheral blood.

Spinal cord injury model

Mice were anesthetized with an intraperitoneal injection of ketamine (100 mg/kg) and xylazine (10 mg/kg). The dorsal surface of the dura mater at the T10 level was exposed by laminectomy, and a moderate (impact force = 60 kdyn) contusion injury was induced using an IH impactor, as reported previously (Cafferty et al., 2004; Glass et al., 2001). The muscles and skin were closed in layers, and the animals were placed in a temperature-controlled chamber until thermoregulation was reestablished. Manual voiding of the bladder was performed twice per day until reflex bladder emptying was reestablished.

Injection of MR16-1 and BrdU

Immediately after SCI, mice were given a single intraperitoneal injection of MR 16-1 (100 μg/g body weight; MR16-1-treated group) or the same volume and concentration of purified rat IgG (ICN/Cappel Ohio; control group). To label the cells that divided after the injury, a sterile solution of bromodeoxyuridine (BrdU; 50 μg/g body weight; Sigma) was injected intraperitoneally immediately after the injury, and then every 24 h for 4 days after SCI (a total of 5 times).

Immunohistochemistry

At 4, 7, 14, and 42 days after SCI, animals in the MR16-1-treated and control groups were deeply anesthetized by inhalation of diethyl ether and transcardially perfused with 4% paraformaldehyde in 0.1 M phosphate-buffered saline (PBS). The spinal cord tissue was removed and post-fixed in 4% paraformaldehyde in PBS for a few hours at room temperature. The tissue samples were immersed in 10% sucrose in PBS at 4 °C for 24 h, then placed in 30% sucrose in PBS for 48 h, and embedded in OTC compound. The embedded tissue was immediately frozen in liquid nitrogen and stored at −80 °C until use. Frozen spinal cord tissues were sectioned on a cryostat at 20 μm, either in the axial or sagittal plane. Luxol fast blue and Oil red O staining were performed to evaluate the spared myelin and myelin debris.

For immunohistochemistry with fluorescent antibodies, spinal cord sections were permeabilized with 0.03% Triton X-100 and 10% normal goat serum in 0.01 M PBS, pH 7.4, for 30 min. The following primary antibodies were applied overnight at 4 °C: rat anti-CD11b, 1:200 (Serotec, Oxford, United Kingdom); rabbit anti-Iba-1, 1:200 (Wako Pure Chemical Industries, Osaka, Japan); rat anti-LAMP2, 1:200 (Abcam, Cambridge, UK); rat anti-Mac2, 1:200 (Cedarlane, Hornby, Ontario); rabbit anti-GFP, 1:500 (MBL, Nagoya, Japan); goat anti-GFP, 1:500 (Rockland Immunochemicals, Gilbertsville, PA); or chick anti-GFP, 1:500 (Aves Lab, Tigard, OR). The sections were then incubated for 1 h at room temperature with secondary antibodies conjugated with Texas red or fluorescein isothiocyanate (FITC; all from Jackson Immunoresearch, West Grove, PA). The sections were then washed, wet-mounted, and examined by epi-fluorescence. Multiple staining with Oil red O was performed by the method reported by Koopman et al. (2001).

For diaminobenzidine (DAB; Sigma) staining, mouse anti-Neurofilament 200kD antibody, 1:200 (Chemicon, Temecula, CA) or goat anti-5HT, 1:200 (Immunostar, Hudson, WI) was used as the primary antibody, followed by horseradish peroxidase (HRP)-labeled goat anti-mouse IgG or donkey anti-goat IgG as the secondary antibody. The staining was visualized with DAB, and the sections were washed, dehydrated, cleared in xylene, and mounted.

Quantitative analyses

For quantitative analyses, three representative midsagittal or axial sections through the injured portion of the spinal cord of each mouse were selected randomly and captured at 50× magnification. The areas of tissue immunopositive for CD11b, Iba-1, LAMP2, Mac2, Neurofilament 200kD, and Nogo-A, and those stained with Oil red O (ORO) and Luxol Fast Blue (LFB) were quantified using the ImageJ software and MCID system (Imaging Research, Inc., St. Catharines, Ontario, Canada). To count the number of macrophages/microglia, three midsagittal sections through the injured portion of the spinal cord of each mouse were selected randomly, and the number of CD11b- or Iba-1- and/or EGFP-immunopositive cells contained within a cephalocaudal stretch of 500 μm at the indicated levels was counted. To confirm the CD11b-Iba-1 double-staining as a marker of macrophages/microglia the ratio of CD11b-Iba-1 double-stained cells to total CD11b-positive cells was also quantified. To count the LAMP2- andMac2-positive cells, three midsagittal sections through the injured portion of the spinal cord of each mouse were selected randomly, and a threshold was determined from the basal fluorescence of a portion of intact tissue. From the epicenter area (0–1-mm caudal and rostral to the epicenter), 15 non-overlapping high-power fields were chosen at random (630× magnification; total area 0.39 mm^2). An immunopositive cell was defined as a cell with staining over 10% of its soma, as determined by the MCID system, and the number of stained and unstained cells was counted manually. For the quantification of $5HT^+$ fibers, five regions (the dorsal horn and ventral horn of both sides, and the site around the central canal) from each axial section of the cord, 2-mm caudal to the epicenter, were captured at ×200 magnification, and the area of the $5HT^+$ tissue in each field was quantified using the MCID system. The light intensity and threshold values were maintained at constant levels for all analyses.

Flow cytometry

Mice were transcardially perfused with 0.1 M phosphate-buffered saline, and the spinal cords were harvested. The injured portion of each spinal cord (6 mm) was surgically dissected, digested with collagenase, mechanically homogenized, and passed through a wire mesh screen (Sigma-Aldrich Canada Ltd., Ontario, Canada) to obtain a single-cell suspension. The cells were washed in PBS containing 3% FBS, and incubated for 5 min on ice with Fc Block and 30 min on ice with fluorescent antibodies. Flow cytometric analysis was performed using a FACS Calibur (Becton Dickinson) and MoFlo (Dakocytomation), and the data were analyzed using Cell Quest software. The cells were stained with antibodies against CD11b-PE, CD45-FITC, and CD45-APC (eBioscience, San Diego, CA), and were classified according to their expression level of CD45 (common leukocyte antigen) and CD11b (complement 3 receptor), with $CD11b^+$ $CD45^{high}$ indicating hematogenous macrophages and $CD11b^+$ $CD45^{low}$ indicating resident microglia, as reported previously (Sedgwick et al., 1991). At least 1.0×10^6 cells were analyzed for each spinal cord sample.

Western blot analysis

Twenty-four hours after the injury, the spinal cord tissue at the lesion epicenter (6 mm in length) was dissected from the mice (four animals per group and four sham-operated animals), homogenized in MAPK lysis buffer containing protease inhibitors, sonicated, and spun at 15,000 rpm. The proteins in the supernatants were separated by 10% SDS-PAGE and transferred to a polyvinylidene difluoride membrane by electrophoresis. The membranes were blocked for 1 h at room temperature in TBST buffer containing 4% non-fat milk, NaCl (150 mM), and 0.05% Tween 20. The blots were then incubated with primary polyclonal rabbit anti-CCL2 antibody (1:2000; Abcam, Cambridge, MA), goat anti-CCL5 antibody, 1:500 (eBioscience, San Diego, CA); rabbit anti-CXCL-10 antibody, 1:500 (Cedarlane, Hornby, Ontario); rabbit anti-GM-CSF antibody, 1:2000 (Abcam, Cambridge, MA); or mouse anti-α-tubulin antibody, 1:500 followed by a secondary HRP-conjugated anti-rabbit, goat, or mouse IgG antibody. The blots were visualized with the ECL Blotting Analysis System (Amersham, Arlington Heights, IL).

Real time RT-PCR

A 4-mm-long spinal cord segment at T10 was collected at the indicated times, the total RNA was isolated using an RNeasy Kit (Qiagen Science, Maryland, USA), and cDNA was obtained by reverse transcription. The cDNA synthesis was performed at 42 °C for 50 min in a final volume of 20 μl, following the manufacturer's instructions for Superscript II RNase H Reverse Transcriptase (Invitrogen). The template cDNA was normalized to the β-actin mRNA. Real time RT-PCR was performed using an Mx3000P thermal cycler (Stratagene) with SYBR green (TaKaRa RR041A). For every set of RT-PCR analyses, at least three independent experiments were performed. The amplification was performed using the following primers: CCL2, sense 5′-GCATCCACGTGTTGGCTCA-3′, antisense 5′-CTCCAGCCTACT-CATTGGGATCA-3′; CCL5, sense 5′-AGATCTCTGCAGCTGCCCTCA-3′, antisense 5′-GGAGCACTTGCTGCTGGTGTAG-3′; CXCL10, sense 5′-TGAATCCGGA ATCTAAGACCATCAA-3′, antisense 5′-AGGACTAGC-CATCCACTGG GTAAAG-3′ (purchased from Takara, Kyoto, Japan) and GM-CSF, sense 5′-AAGGTCCTGAGGAGGA TGTG-3′, antisense 5′-GAGGTTCAGGGCTTCTTTGA-3′ (purchased from Hokkaido System Science, Sapporo, Japan).

Statistical analysis

Values are reported as the mean ± SEM. Statistical significance was analyzed using the unpaired Student's *t*-test, and significance was accepted at $P<0.05$.

Results

Anti-IL-6 receptor antibody treatment reduced inflammatory cell accumulation

To examine the effect of MR16-1 on the infiltration of inflammatory cells after SCI, immunostaining for CD11b and Iba-1 was performed. Although CD11b is known to be expressed by granulocytes and some T cells, 93.6 ± 3.3% of the infiltrated cells were CD11b and Iba-1 double-positive at 4, 7, and 14 days post-injury (dpi), indicating that the immunocompetent cells present at the injured site at those times after SCI were mostly hematogenous macrophages and resident microglia (Figs. 1A–E). While the CD11b-positive area increased in both the MR16-1 and control groups, with a peak at 7 dpi, the MR16-1-treated animals showed a significantly smaller $CD11b^+$ area compared to the control animals: a non-significant difference at 4 and 7 dpi that developed to a significant difference at 14 dpi (Fig. 1F). These findings suggest that MR16-1 administration reduced the accumulation of $CD11b^+$ cells at the late stage of inflammation, even though MR16-1 was only administered once, at the acute stage.

To determine whether the administration of MR16-1 alters the subtype of $CD11b^+$ cells at the acute stage, the profiles of the recruited $CD11b^+$ cells were analyzed using flow cytometry. Homogenates of the injured spinal cord were analyzed to determine the ratio of hematogenous macrophages to total $CD11b^+$ cells. We first confirmed that within the $CD11b^+$ population, hematogenous macrophages could be distinguished from the resident microglia by their expression level of CD45, as reported previously (Sedgwick et al., 1991). At 4 dpi, 37.6 ± 3.9% of the $CD11b^+$ cells were $CD45^{high}$ hematogenous macrophages in the control group, whereas only 22.3 ± 2.9% of these cells were $CD45^{high}$ in the MR16-1-treated group. Although the proportion of hematogenous macrophages had increased in both groups at 7 dpi, the difference in their proportions between the MR16-1-treated and control mice was significant (57.8 ± 1.9% in the control group, 41.0 ± 2.2% in the MR16-1-treated group) (Figs. 1G–I). MR16-1 treatment thus reduced the relative abundance of hematogenous macrophages in the injured spinal cord.

MR16-1 treatment caused the central player in the inflammation after SCI to shift from hematogenous macrophages to resident microglia

To determine whether MR16-1 specifically affects the recruitment of hematogenous macrophages into the injured spinal cord, contusive SCI was induced in chimeric mice, which were generated by irradiating

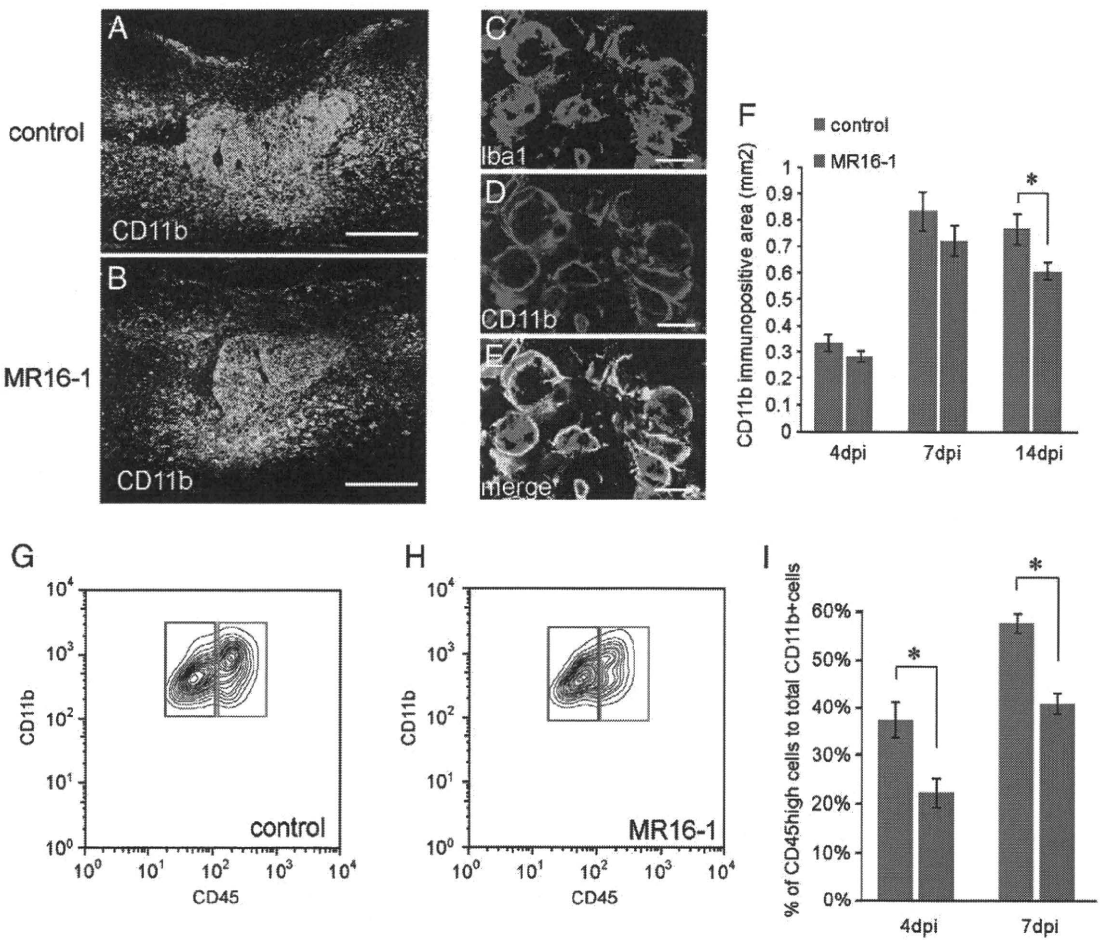

Fig. 1. MR16-1 treatment accelerates the resolution of inflammation. A, B, F: There was a significant difference in the $CD11b^+$ area between the control group (A) and the MR16-1-treated group (B) at 14 dpi, but not at 4 or 7 dpi (F). C–E: 96.9 ± 1.3% of the $CD11b^+$ cells (D) were double-labeled with Iba1 (C, E), indicating that the accumulated $CD11b^+$ cells were inflammatory macrophages/microglia. G–I: MR16-1-treatment decreased the proportion of hematogenous macrophages in the injured spinal cord at 4 and 7 dpi. Hematogenous macrophages ($CD11b^+CD45^{high}$, blue box) and microglia ($CD11b^+CD45^{low}$, red box) were identified according to their levels of CD11b and CD45 expression. I: The proportion of hematogenous macrophages within the $CD11b^+$ population was significantly lower in the MR16-1-treated animals than in the control group at 4 and 7 dpi. Values are means ± SEM. *$P<0.05$. Scale bars = 500 μm in A, B; 20 μm in C–E.

recipient mice and then transplanting purified EGFP-expressing HSCs into them (Matsuzaki et al., 2004). Flow cytometric analysis revealed that 3 months after the HSC transplantation, 88.34 ± 1.45% of the CD11b$^+$ leukocytes in the blood of the chimeric mice were EGFP-positive. In contrast, only 1.57% of the CD11b$^+$ cells in the uninjured spinal cord expressed EGFP, suggesting that the recruitment of microglia from the hematopoietic pool was a rare event. Since the irradiation dose required for this method is rather high (10.5 Gy), which could affect microglial turnover (Mildenberger et al., 1990), we quantified the accumulation of CD11b+ cells at the lesion of chimeric mice, and compared it to that of wild-type mice. There was no significant difference in the number of CD11b+ cells between the chimeric mice and wild-type mice at 4, 7, or 14 dpi ($P = 0.60$, 0.76, 0.67, respectively). This result is consistent with the previous report by Turrin et al. (2007), which showed that the chimerization with 10 Gy irradiation dose does not significantly affect the acute inflammatory response. Thus, these chimeric mice enabled us to distinguish in situ hematogenous macrophages from endogenous microglia by their EGFP immunoreactivity (Figs. 2A–C), and examine the precise spatio-temporal localization of these cell populations after SCI.

Consistent with our findings using wild-type mice, the total number of recruited CD11b$^+$ macrophages/microglia was comparable between the MR16-1-treated and control groups at 4 dpi (not shown), but the proportion and distribution of the hematogenous macrophages and microglia were completely different (Figs. 2D, E, G, and I). In the MR16-1-treated group, there were significantly fewer CD11b$^+$EGFP$^+$ hematogenous macrophages at the lesion site (Fig. 2G), and there were significantly more CD11b$^+$EGFP$^-$ resident microglia, especially in areas 1.0- to 2.0-mm away from the lesion site (Fig. 2I). Thus, at 4 dpi, the MR16-1 treatment led to a reduced accumulation of hematogenous macrophages at the lesion epicenter, and an increased number of microglia at sites rostral and caudal to the lesion epicenter.

Similarly, at 7 dpi, although the distribution of CD11b$^+$ cells was comparable in the control and MR16-1-treated groups (Fig. 2F), the composition of the CD11b$^+$ population was dramatically different. In the MR16-1-treated group, the CD11b$^+$EGFP$^+$ hematogenous macrophage accumulation at the lesion epicenter was significantly reduced (Fig. 2H), and the CD11b$^+$EGFP$^-$ resident microglia had significantly increased (Fig. 2J). These results indicate that the central player in the inflammation after SCI shifted from being hematogenous macrophages to being resident microglia, following MR16-1-treatment.

MR16-1 treatment reduced the expression of macrophage-recruiting chemokines and increased the GM-CSF level at the lesion site

Although there is no evidence that IL-6 directly stimulates the infiltration or proliferation of inflammatory cells, it does affect the expression of various cytokines; furthermore, the blockade of IL-6 signaling during inflammation causes a drastic change in the cytokine profile, including the chemokines and colony-stimulating factors (CSFs) (Matsumura et al., 1999; Romano et al., 1997). Because the infiltration of hematogenous macrophages is mediated by chemokines (Babcock et al., 2003; Romano et al., 1997) and the increased proliferation of microglia is mainly controlled by CSFs (Giulian and Ingeman, 1988; Lee et al., 1994), we examined the expression levels of CCL2 (MCP-1), CCL5 (RANTES), CXCL10 (IP-10), and GM-CSF, which are representative cytokines known to direct cell infiltration and proliferation, by quantitative real time PCR, 12 h after injury. The mRNA levels of CCL2, CCL5, and CXCL10 were significantly attenuated by MR16-1-administration compared to the control group (to 15.0%, 49.7% and 30.8% of the control levels, respectively), whereas the GM-CSF mRNA level was significantly increased (to 214% of the control level) (Figs. 3A–D). We also quantified the cytokine proteins by western blotting. The protein level of CCL2 was significantly decreased (to 80.7% of the control level), whereas the GM-CSF level was significantly increased (to 193% of the control level). Although the difference did not reach to statistical significance, we also observed a tendency for the protein levels of CCL5 and CXCL10 to decrease (Figs. 3E–H).

Microglia had higher phagocytic capacities than hematogenous macrophages

To determine whether the shift in the major inflammatory cells by MR16-1 treatment affected the inflammatory process, we further characterized the hematogenous macrophages and the microglia. The phagocytosis of tissue debris by inflammatory cells is a pivotal process for spinal cord repair after injury, as the debris includes various cytotoxic agents and axonal growth inhibitory factors. Quantitative analysis revealed that the expression of LAMP2, a marker for endosomes/lysosomes, was significantly increased at the lesion epicenter in the MR16-1-treated group compared to the control group, at 4, 7, and 14 dpi (Figs. 4A–C). Previous reports showed that the resident microglia have higher phagocytic activity than the infiltrating hematogenous macrophages (Rinner et al., 1995; Schilling et al., 2005). Consistent with these reports, we found that significantly more Iba1$^+$EGFP$^-$ resident microglia expressed LAMP2 than did the Iba1$^+$EGFP$^+$ hematogenous macrophages at 4 and 7 dpi (Figs. 4D–G).

In addition, we performed immunostaining with Mac2, which is reported to participate in the phagocytosis of myelin (Rotshenker et al., 2008). Although Mac2 was expressed on the cell membrane of most of the accumulated cells, only a portion of the macrophages/microglia expressed Mac2 in their cytoplasm. Consistent with the LAMP2 results, more of the Iba1$^+$EGFP$^-$ resident microglia than Iba1$^+$EGFP$^+$ hematogenous macrophages showed cytoplasmic expression of Mac2 (Figs. 5A–D, and I). Similarly, the average size and intracellular Mac2$^+$ area of the resident microglia were significantly greater at 7 dpi than those of hematogenous macrophages (Figs. 5J and K). We also performed triple staining for Iba-1, EGFP, and Oil red O using the method reported by Koopman et al. (2001) to observe phagocytosed lipid, which is derived from myelin. The Oil red O$^+$ area in each cell body was significantly greater in the Iba1$^+$EGFP$^-$ resident microglia than in the Iba1$^+$EGFP$^+$ hematogenous macrophages, and was increased at 7 dpi by the MR16-1 treatment (Figs. 5E–H, L).

MR16-1 treatment promotes repair of the spinal cord

To examine the effect of the altered inflammatory response on spinal cord repair, we evaluated the clearance of myelin debris by Oil red O staining and Nogo-A immunostaining, as well as the sparing of myelin sheath, which is evaluated by Luxol Fast Blue staining. At 14 and 42 dpi, the Oil red O$^+$ area was significantly decreased in the MR16-1-treated group compared to the control group (Figs. 6A–C). The deposition of Nogo-A, the major myelin-derived axonal growth inhibitor, was also decreased by MR16-1 treatment (Figs. 6D–F). Furthermore, we evaluated the spared myelin sheath using Luxol fast blue staining. At the lesion epicenter, the area of the spared myelin sheath in the MR16-1-treated group was significantly greater than in the control group at 14 and 42 dpi (Figs. 6G–I).

To determine the effect of MR16-1 on repair of neural tissue, we quantified the RT-97$^+$ (Neurofilament 200kD) fibers at the lesion epicenter and the 5-HT$^+$ (serotonergic) fibers that were caudal to the lesion site. There was no significant difference in the area of RT-97$^+$ fibers between the two groups at 14 dpi, but a significantly larger RT-97$^+$ area was observed in the MR16-1-treated group at 42 dpi (Figs. 6J–K). Similarly, there was no significant difference in the 5-HT$^+$ area between the two groups at 14 dpi. Although there was a slight increase in 5-HT$^+$ fibers at 42 dpi, even in the control group, which is characteristic of contusive SCI, a significantly larger area of 5-HT$^+$

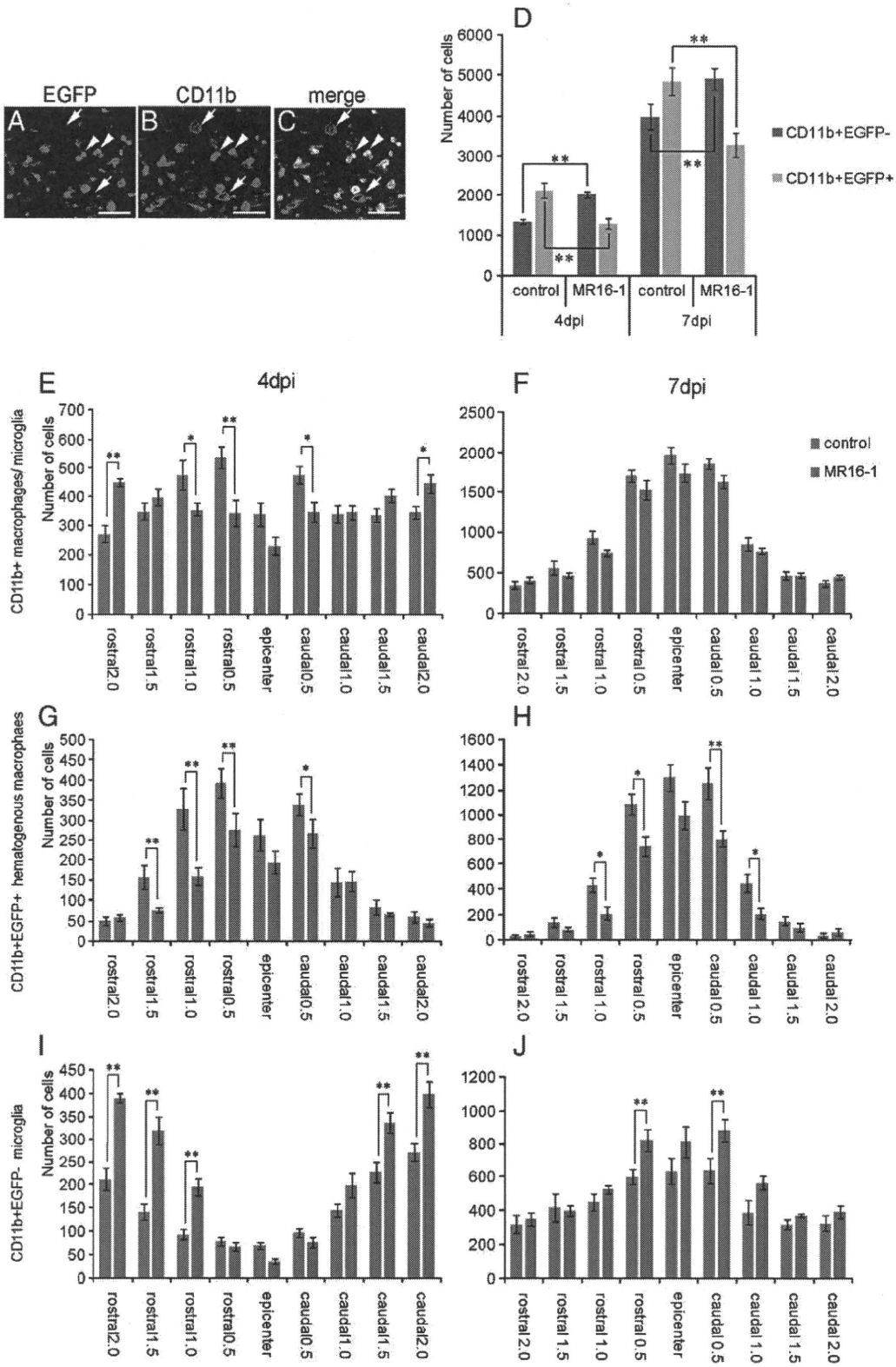

Fig. 2. MR16-1 treatment switches the major inflammatory cell type, from hematogenous macrophages to resident microglia. Analysis using chimeric mice. A–C: Immunostaining for EGFP (A, green) and CD11b (B, red), showing the distribution of $CD11b^+EGFP^+$ hematogenous macrophages (arrowheads) and $CD11b^+$ $EGFP^-$ resident microglia (arrows) in the injured spinal cord (C, merged). D: In the MR16-1-treated group, the major player in the inflammation switched from $CD11b^+EGFP^+$ hematogenous macrophages (light gray) to $CD11b^+EGFP^-$ resident microglia (dark gray) at 4 and 7 dpi. Number and distribution of macrophages/microglia in the spinal cord at 4 and 7 dpi. E, F: MR16-1 did not significantly affect the total number of inflammatory cells ($Cd11b^+$) at 4 (E) or 7 (F) dpi. G, H: MR16-1 reduced the recruitment of $CD11b^+EGFP^+$ hematogenous macrophages at 4 (G) and 7 (H) dpi. I, J: MR16-1 treatment increased the number of $CD11b^+EGFP^-$ resident microglia 1.0 to 2.0 mm rostral and caudal to the lesion epicenter at 4 dpi (I). At 7 dpi, both groups showed a shift in $CD11b^+EGFP^-$ microglia to the lesion epicenter, where the number of $CD11b^+EGFP^-$ microglia was significantly higher in the MR16-1-treated animals (J). Values are means ± SEM. $^*P<0.05$. $^{**}P<0.01$. Scale bars = 50 μm in A–C.

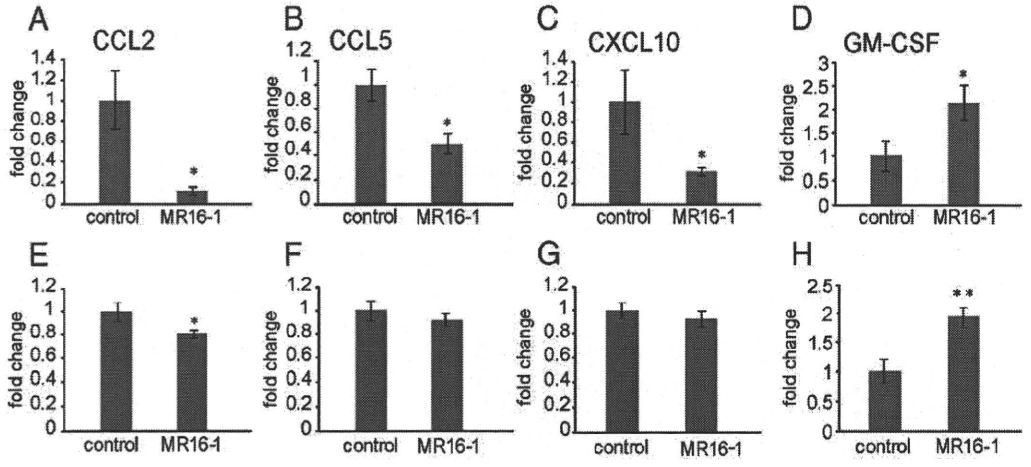

Fig. 3. MR16-1 decreases the expression level of macrophage-recruiting chemokines, while increasing that of GM-CSF. A–D: The CCL2 (A), CCL5 (B), CXCL10 (C), and GM-CSF (D) mRNA expression levels in the spinal cord tissue 12 h after injury were determined using quantitative RT-PCR. Macrophage-recruiting chemokines had significantly decreased, while the expression of GM-CSF, a known mitogen for microglia, had increased. E–H: The protein levels of the CCL2(E), CCL5(F), CXCL10(G) and GM-CSF(H) 24 h after injury were determined by western blot analysis. The protein level of CCL2 (E) was significantly decreased, whereas the GM-CSF (H) level was significantly increased. There was a tendency for the protein levels of CCL5 (F) and CXCL10 (G) to decrease, although the change was not statistically significant. Values are means ± SEM. $^{*}P<0.05$.

fibers was observed in the MR16-1-treated group than in the control group (Figs. 6M–O).

Discussion

IL-6 is a pro-inflammatory cytokine that triggers secondary injury in the pathophysiology of SCI. IL-6 binds to soluble and membrane-bound IL-6-receptor to form a complexed ligand for gp130, the common signal transducer of IL-6 and its related cytokines. MR16-1 is a neutralizing antibody for IL-6-receptor that competitively inhibits its binding to IL-6, thereby blocking IL-6-receptor-mediated cell signaling. We previously reported that the systemic administration of MR16-1 decreases the phosphorylation of signal transducer and activator of transcription 3 (STAT3) in the injured spinal cord, demonstrating that this treatment potently affects the IL-6/JAK/STAT3 signaling pathway. Subsequently, we showed that MR16-1 administration after SCI reduces the number of inflammatory cells present 2 weeks after injury and decreases the amount of reactive astrogliosis, leading to improved functional recovery (Okada et al., 2004). Our present study extends these findings, showing that MR16-1 treatment alters the nature of the inflammatory response after SCI.

Here we found that the temporary inhibition of IL-6 signaling by MR16-1 treatment caused a significant reduction in the macrophage/microglia accumulation at 14 dpi, but not at 4 or 7 dpi. We had expected MR16-1 to have an anti-inflammatory effect, because IL-6 is a pro-inflammatory cytokine, so it was unclear why the immediate administration of MR16-1 affected only the late phase of the inflammatory response after SCI. We hypothesize that the response was delayed because the effects of MR16-1 treatment were owed to changes in the nature of the inflammatory response, rather than to the immediate effects of inhibiting the IL-6 signal.

Previous studies showed that functional recovery after SCI is affected by the properties of the inflammatory response, which are determined by the cell types involved and their state of activation (Gris et al., 2004; Popovich et al., 1999; Rapalino et al., 1998; Saville et al., 2004; Schwartz et al., 1999). Hematogenous macrophages and microglia are the major players in the inflammatory pathology of SCI, and their characteristics have therefore been of major interest. Of the two, hematogenous macrophages are regarded as more detrimental, because removing them or preventing their infiltration into the injured tissue reduces the degree of secondary injury and improves functional recovery (Gris et al., 2004; Popovich et al., 1999). In contrast, microglia are believed to be relatively beneficial for spinal cord repair, owing to their higher phagocytotic activity and expression of various neurotrophic factors (Lalancette-Hebert et al., 2007; Schilling et al., 2005). The state of cell activation also affects the nature of the inflammation; the implantation of bone marrow-derived macrophages previously stimulated by co-incubation with peripheral nerve or skin improves spinal cord repair (Bomstein et al., 2003; Rapalino et al., 1998).

Because IL-6 has a leading role in recruiting macrophages during inflammation, we hypothesized that MR16-1 treatment would decrease the infiltration of hematogenous macrophages. Therefore, we focused on the balance between the types of inflammatory cells, i.e., the hematogenous macrophages and microglia. Flow cytometric analysis revealed that the proportion of infiltrated $CD45^{high}$ hematogenous macrophages decreased markedly following MR16-1 treatment, with the result that resident microglia replaced hematogenous macrophages as the major inflammatory cell type at the lesion site. Furthermore, we performed quantitative analyses in chimeric mice bearing transplanted EGFP-expressing, highly purified HSCs. These analyses showed that, besides the reduced infiltration of hematogenous macrophages following MR16-1 treatment, the number of resident microglia increased, contributing to the shift in the major inflammatory cell type. The increase in the number of BrdU+ microglia by MR16-1 indicated that the higher number of microglia might have resulted from their increased proliferation (Suppl. Fig. 1).

Two mechanisms appear to mediate this phenomenon. First, the number of hematogenous macrophages is reduced because fewer are recruited from the blood pool. Various chemokines are known to mediate macrophage infiltration; in particular, CCL2, CCL5, and CXCL10 have a demonstrated role in recruiting macrophages following CNS injury (Babcock et al., 2003; Ghirnikar et al., 1998; Glass et al., 2001; Liu et al., 2001). Here we observed decreased expression levels of CCL2, CCL5, and CXCL10 following MR16-1-treatment, which could account for the reduced infiltration of hematogenous macrophages. This agrees with the observation that IL-6 is a major player in directing chemokine-mediated macrophage infiltration during inflammation (Hurst et al., 2001; Romano et al., 1997).

In contrast to hematogenous macrophage recruitment, microglial proliferation is mainly regulated by colony-stimulating factors (CSFs) (Giulian and Ingeman, 1988; Lee et al., 1994), and the local increase in GM-CSF that we observed could have stimulated their proliferation, resulting in their increased numbers at the lesion site (Lee et al., 1994). Since IL-6, like other cytokines, interacts with various other

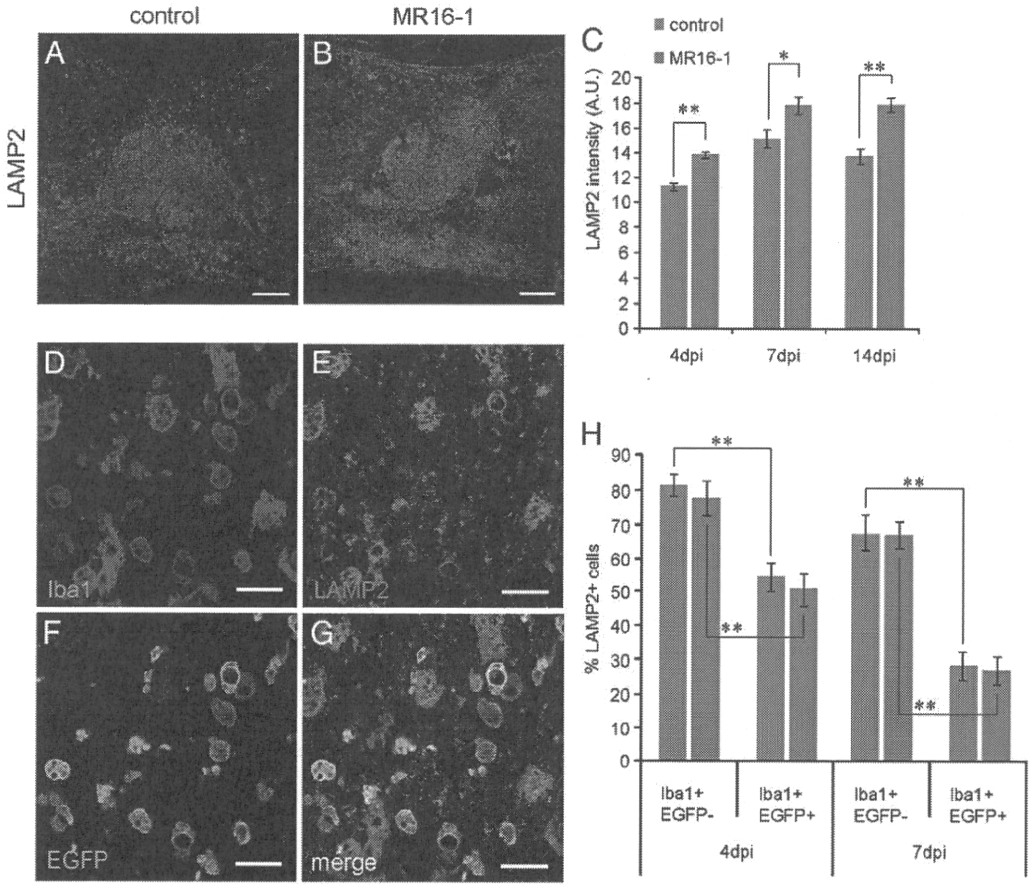

Fig. 4. MR16-1 enhances the phagocytotic activity in the injured spinal cord. A–C: Phagocytosis, indicated by LAMP2 expression, was increased by MR16-1-treatment. D–H: Quantification of the LAMP2$^+$ inflammatory subsets in injured chimeric mice indicated that the microglia had significantly higher phagocytotic activity than the hematogenous macrophages. MR16-1-treatment did not affect the phagocytotic activity of either cell subpopulation. Values are means ± SEM. *P<0.05. Scale bars = 200 μm in A, B; 20 μm in D–G.

cytokines or neurotrophic factors, and since previous reports show that the inhibition of IL-6 signaling drastically alters the expression profiles of various cytokines (Matsumura et al., 1999; Romano et al., 1997), the temporary inhibition of IL-6 signaling may, by altering the chemical milieu, underlie the shift in the dominant inflammatory cell type following MR16-1 treatment.

Given the characteristics of hematogenous macrophages vs. those of resident microglia, the MR16-1-induced switch in the central player in post-SCI inflammation should be beneficial. The evidence bears out this prediction. In the injured spinal cord, broad destruction of the blood–spinal cord barrier (BSCB) permits the infiltration of hematogenous macrophages into the lesion. If the infiltrating neutrophils and macrophages are depleted or blocked, tissue sparing improves, as does axonal regeneration/sprouting (Gris et al., 2004; Popovich et al., 1999; Saville et al., 2004). The cytotoxicity of hematogenous macrophages may be due to their increased NO production in the injured CNS (Ponomarev et al., 2007). In addition, a recent report showed that direct physical interactions between activated hematogenous macrophages and axons causes the axons to retract; microglia have a similar effect, but it is much weaker (Horn et al., 2008).

Despite the detrimental effects of hematogenous macrophages, the accumulation of inflammatory cells is considered to be critical for the repair process, because these cells clear away tissue debris and release neurotrophic factors. Previous studies demonstrated that the resident microglia play an active role in repairing the injured CNS, through their relatively high phagocytotic activity (Schilling et al., 2005) and by releasing various neuroprotective cytokines or neurotrophic factors (Lalancette-Hebert et al., 2007; Lambertsen et al., 2009). In fact, the tissue debris within the injured spinal cord contains myelin-derived axonal growth inhibitory factors (Bregman et al., 1995; Merkler et al., 2001) that hinder the repair process after SCI, so clearing away this debris is prerequisite for axonal re-growth.

In this study, MR16-1 treatment led to an increased accumulation of microglia, which expressed higher levels of the phagocytic markers LAMP2 and Mac2 than did the hematogenous macrophages. Furthermore, the Oil red O-stained intracellular area of microglial cells was greater than that of hematogenous macrophages. These data indicate that the microglia had higher phagocytotic activity than the hematogenous macrophages, and this activity was enhanced by the MR16-1 treatment.

The enhanced phagocytosis by MR16-1 treatment, along with attenuation of injury, resulted in decreased Oil red O staining (indicating reduced deposition of myelin) and decreased immunostaining for the axonal growth inhibitor Nogo-A, at the chronic phase of post-SCI inflammation. These effects could have contributed to the formation of a permissive environment for the regeneration or sprouting of neuronal fibers. In fact, the process of spinal cord repair seemed to be enhanced, given the increase in the RT-97$^+$ fibers and 5HT$^+$ serotonergic fibers between 14 and 42 dpi. The higher density of RT-97 fibers in the penumbral area in the treated group, and the lack of RT-97+ fibers at the center of the injury site in both groups, may indicate that enhanced sprouting contributed to the increase in 5HT+ fibers caudal to the lesion site (Supplemental Fig. 2).

Taken together, it is possible that the immediate administration of MR16-1 affected only the late phase of inflammation, because the change in cytokine profile by MR16-1 enhanced the participation of microglia in the inflammatory process, resulting in a tissue-protective inflammation. Our results with LFB, Oil red O, and immunostaining for

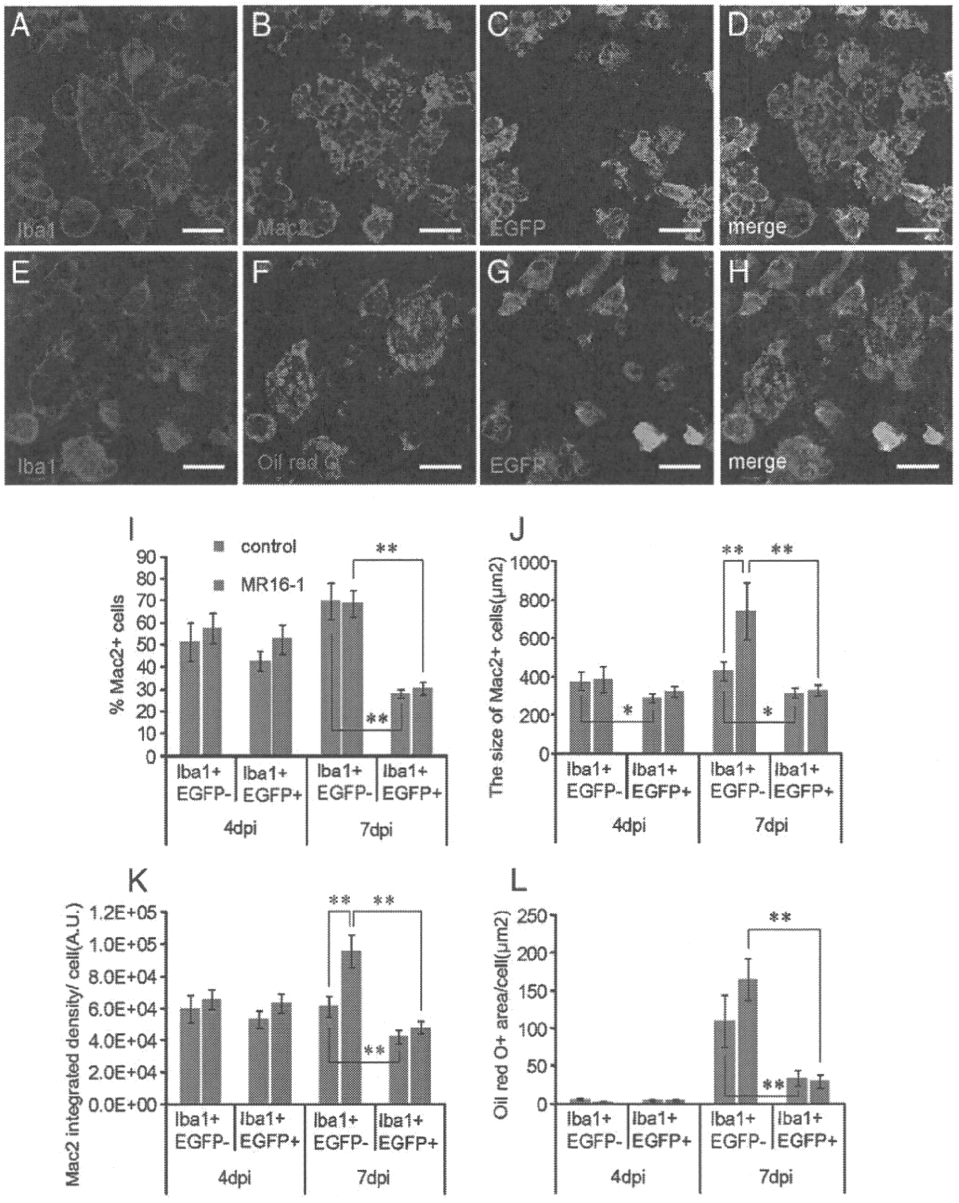

Fig. 5. Microglia have higher phagocytic activity against myelin debris than hematogenous macrophages. A–D: Mac2 expression was observed in the cells at the lesion epicenter. A portion of the macrophages/microglia expressed Mac2 in their cytoplasm. E–H: Oil red O^+ particles were observed in the cell body of macrophages/microglia at the lesion epicenter. I: The cytoplasmic expression of Mac2 was greater in $Iba1^+EGFP^-$ resident microglia than in $Iba1^+EGFP^+$ hematogenous macrophages. J, K: The average size (J) and Mac2-integrated density (K) at 7 dpi of each $Iba1^+EGFP^-$ resident microglial cell were significantly greater than those of $Iba1^+EGFP^+$ hematogenous macrophages, and were increased by MR16-1 treatment. The intracellular Oil red O-stained area was significantly greater in the $Iba1^+EGFP^-$ resident microglia than in the $Iba1^+EGFP^+$ hematogenous macrophages, and this tendency was increased at 7 dpi by MR16-1 treatment (L). Values are means ± SEM. $^*P<0.05$. $^{**}P<0.01$. Scale bars = 20 μm in A–H.

Nogo-A, which showed reduced injury and deposition of debris, support this idea. This series of immune responses takes place over a long time, which is consistent with the effects of MR16-1 treatment appearing only at the late phase.

However, despite the marked improvement in the inflammatory response obtained with MR16-1 treatment, skepticism about the therapeutic effects of IL-6 signal inhibition remains, because several studies have shown that IL-6 signaling has neuroprotective functions after CNS trauma. For example, Penkowa et al. showed that the overexpression of IL-6 results in decreased oxidative stress and apoptosis, leading to faster tissue repair after brain injury (Penkowa et al., 2003), and IL-6-deficient mice show a slower rate of recovery and healing after brain injury than wild-type mice (Swartz et al., 2001).

Although our results may seem to conflict with these reports, we believe that the apparent discrepancies are owing to the context-dependent pleiotropic actions of IL-6. Our present data revealed that the therapeutic effect of MR16-1 was achieved by inhibiting the excessive infiltration of hematogenous macrophages through the damaged BSCB, during the acute phase of SCI. This idea is corroborated by previous reports demonstrating that the overexpression of IL-6 family cytokines during the acute phase of SCI significantly increases inflammatory cell accumulation, resulting in greater damage (Kerr and Patterson, 2004; Lacroix et al., 2002). On the other hand, IL-6 can enhance spinal cord repair by modifying the migration of reactive astrocytes (Okada et al., 2006) or enhancing axonal re-growth (Miao et al., 2006), and IL-6's temporary inhibition may have little effect on these functions, because astrocyte migration and axonal re-growth are rather long-term processes. Although numerous studies have shown that the recruitment of inflammatory cells aggravates secondary injury after SCI (Ghirnikar et al., 2001; Hausmann, 2003;

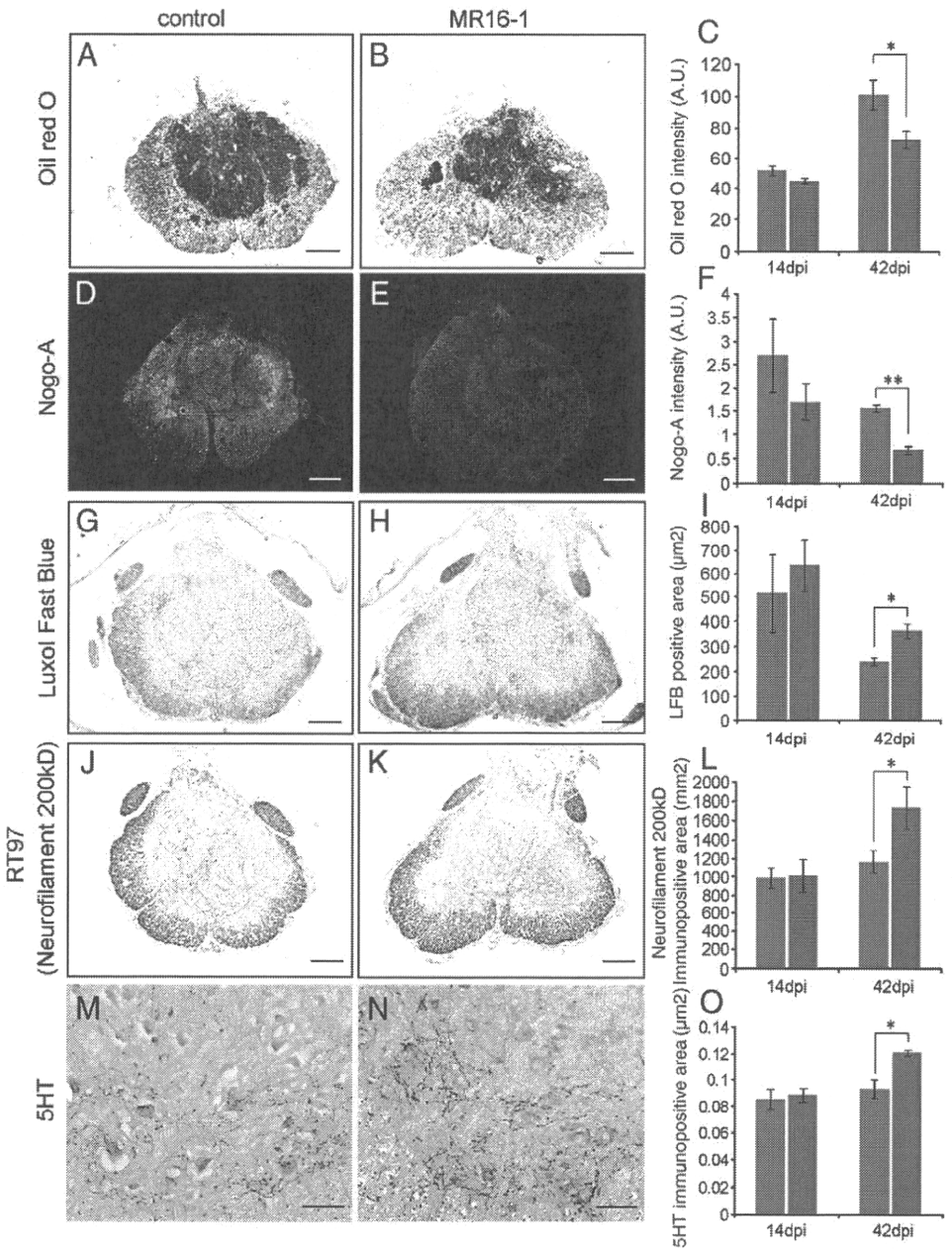

Fig. 6. MR16-1 treatment improves repair of the spinal cord. A–C: MR16-1 treatment improved the clearance of myelin debris, as seen by a significant reduction in the Oil red O-stained area. D–F: The deposition of Nogo-A was decreased in the MR16-1-treated group. G–I: The area of Luxol Fast Blue-stained tissue, which represents spared myelin sheath, was significantly increased by the MR16-1 treatment. J–L: RT-97^{+} (Neurofilament 200kD) fibers at the lesion epicenter were significantly increased in the MR16-1-treated animals at 42 dpi. M–O: 5HT-positive fibers at the ventral horn. 5HT-immunostaining of the area 2 mm caudal to the lesion revealed a significant increase in 5HT^{+} fibers at 42 dpi by the MR16-1-treatment. *$P<0.05$. Scale bars = 200 μm in A, B, D, E, G, H; 50 μm in J, K.

Saville et al., 2004), inflammation itself is important for spinal cord repair (Donnelly and Popovich, 2008), and excessive suppression of the inflammatory response can be detrimental. In the present study, we showed that anti-IL-6-receptor antibody treatment at the acute stage of injury switches the main subpopulation of inflammatory cells from hematogenous macrophages to microglia, which does not simply suppress inflammation: rather, it changes the characteristics of the post-traumatic inflammation to promote spinal cord repair.

Given that a humanized antibody for the human IL-6 receptor (MRA; tocilizumab) is already in clinical use (Choy et al., 2002; Nishimoto et al., 2000; Sato et al., 1993), the present data support the potential application of the anti-IL-6-receptor antibody for the treatment of SCI. However, in most clinical situations, it is not possible to administer an antibody immediately after SCI. Further investigation to determine the therapeutic time window will be needed before this treatment can be tried clinically. Nevertheless, these findings shed light on IL-6's role in the pathology of SCI, and suggest a new approach for SCI treatment, in which the characteristics of inflammation are adjusted to support spinal cord repair, by modifying the cytokine-mediated cellular response.

Author contributions

M.M., M.N., Y.T., M.L. and H.O. designed the research; M.M., O.Y., A. I., T.I., F.RM. and O.T. performed the in vivo experiments; S.M. and Y.M. generated the chimeric mice; Y.O. supplied the anti-IL-6 receptor antibody and analyzed the antibody results; M.M., M.N., S.O., F.RM. and H.K. analyzed the data; M.M., M.N. and H.O. wrote the paper; M.N. and H.O. supervised all the experiments.

Acknowledgments

This work was supported by grants from the Project for the Realization of Regenerative Medicine from the Ministry of Education, Culture, Sports, Science and Technology (MEXT), Japan to H.O.; the General Insurance Association of Japan to M.N., A.I. and Y.T.; and a Grant-in-Aid for the Global COE Program from MEXT to Keio University. This work was also supported by grants from the Grant of Orthopaedics and Traumatology Foundation, Inc. No. 0178 to A.I. We are grateful to Professor Claude Bernard at Monash University for his critical reading of the manuscript.

Appendix A. Supplementary data

Supplementary data associated with this article can be found, in the online version, at doi:10.1016/j.expneurol.2010.04.020.

References

Babcock, A.A., Kuziel, W.A., Rivest, S., Owens, T., 2003. Chemokine expression by glial cells directs leukocytes to sites of axonal injury in the CNS. J. Neurosci. 23, 7922–7930.

Bomstein, Y., Marder, J.B., Vitner, K., Smirnov, I., Lisaey, G., Butovsky, O., Fulga, V., Yoles, E., 2003. Features of skin-coincubated macrophages that promote recovery from spinal cord injury. J. Neuroimmunol. 142, 10–16.

Bregman, B.S., Kunkel-Bagden, E., Schnell, L., Dai, H.N., Gao, D., Schwab, M.E., 1995. Recovery from spinal cord injury mediated by antibodies to neurite growth inhibitors. Nature 378, 498–501.

Cafferty, W.B., Gardiner, N.J., Das, P., Qiu, J., McMahon, S.B., Thompson, S.W., 2004. Conditioning injury-induced spinal axon regeneration fails in interleukin-6 knock-out mice. J. Neurosci. 24, 4432–4443.

Choy, E.H., Isenberg, D.A., Garrood, T., Farrow, S., Ioannou, Y., Bird, H., Cheung, N., Williams, B., Hazleman, B., Price, R., Yoshizaki, K., Nishimoto, N., Kishimoto, T., Panayi, G.S., 2002. Therapeutic benefit of blocking interleukin-6 activity with an anti-interleukin-6 receptor monoclonal antibody in rheumatoid arthritis: a randomized, double-blind, placebo-controlled, dose-escalation trial. Arthritis Rheum. 46, 3143–3150.

Donnelly, D.J., Popovich, P.G., 2008. Inflammation and its role in neuroprotection, axonal regeneration and functional recovery after spinal cord injury. Exp. Neurol. 209, 378–388.

Gensel, J.C., Nakamura, S., Guan, Z., van Rooijen, N., Ankeny, D.P., Popovich, P.G., 2009. Macrophages promote axon regeneration with concurrent neurotoxicity. J. Neurosci. 29, 3956–3968.

Ghirnikar, R.S., Lee, Y.L., Li, J.D., Eng, L.F., 1998. Chemokine inhibition in rat stab wound brain injury using antisense oligodeoxynucleotides. Neurosci. Lett. 247, 21–24.

Ghirnikar, R.S., Lee, Y.L., Eng, L.F., 2001. Chemokine antagonist infusion promotes axonal sparing after spinal cord contusion injury in rat. J. Neurosci. Res. 64, 582–589.

Giulian, D., Ingeman, J.E., 1988. Colony-stimulating factors as promoters of ameboid microglia. J. Neurosci. 8, 4707–4717.

Glass, W.G., Liu, M.T., Kuziel, W.A., Lane, T.E., 2001. Reduced macrophage infiltration and demyelination in mice lacking the chemokine receptor CCR5 following infection with a neurotropic coronavirus. Virology 288, 8–17.

Gris, D., Marsh, D.R., Oatway, M.A., Chen, Y., Hamilton, E.F., Dekaban, G.A., Weaver, L.C., 2004. Transient blockade of the CD11d/CD18 integrin reduces secondary damage after spinal cord injury, improving sensory, autonomic, and motor function. J. Neurosci. 24, 4043–4051.

Hashimoto, M., Nitta, A., Fukumitsu, H., Nomoto, H., Shen, L., Furukawa, S., 2005. Involvement of glial cell line-derived neurotrophic factor in activation processes of rodent macrophages. J. Neurosci. Res. 79, 476–487.

Hausmann, O.N., 2003. Post-traumatic inflammation following spinal cord injury. Spinal Cord 41, 369–378.

Horn, K.P., Busch, S.A., Hawthorne, A.L., van Rooijen, N., Silver, J., 2008. Another barrier to regeneration in the CNS: activated macrophages induce extensive retraction of dystrophic axons through direct physical interactions. J. Neurosci. 28, 9330–9341.

Hurst, S.M., Wilkinson, T.S., McLoughlin, R.M., Jones, S., Horiuchi, S., Yamamoto, N., Rose-John, S., Fuller, G.M., Topley, N., Jones, S.A., 2001. Il-6 and its soluble receptor orchestrate a temporal switch in the pattern of leukocyte recruitment seen during acute inflammation. Immunity 14, 705–714.

Kawamoto, S., Niwa, H., Tashiro, F., Sano, S., Kondoh, G., Takeda, J., Tabayashi, K., Miyazaki, J., 2000. A novel reporter mouse strain that expresses enhanced green fluorescent protein upon Cre-mediated recombination. FEBS Lett. 470, 263–268.

Kerr, B.J., Patterson, P.H., 2004. Potent pro-inflammatory actions of leukemia inhibitory factor in the spinal cord of the adult mouse. Exp. Neurol. 188, 391–407.

Klusman, I., Schwab, M.E., 1997. Effects of pro-inflammatory cytokines in experimental spinal cord injury. Brain Res. 762, 173–184.

Koide, Y., Morikawa, S., Mabuchi, Y., Muguruma, Y., Hiratsu, E., Hasegawa, K., Kobayashi, M., Ando, K., Kinjo, K., Okano, H., Matsuzaki, Y., 2007. Two distinct stem cell lineages in murine bone marrow. Stem Cells 25, 1213–1221.

Koopman, R., Schaart, G., Hesselink, M.K., 2001. Optimisation of oil red O staining permits combination with immunofluorescence and automated quantification of lipids. Histochem. Cell Biol. 116, 63–68.

Lacroix, S., Chang, L., Rose-John, S., Tuszynski, M.H., 2002. Delivery of hyper-interleukin-6 to the injured spinal cord increases neutrophil and macrophage infiltration and inhibits axonal growth. J. Comp. Neurol. 454, 213–228.

Lalancette-Hebert, M., Gowing, G., Simard, A., Weng, Y.C., Kriz, J., 2007. Selective ablation of proliferating microglial cells exacerbates ischemic injury in the brain. J. Neurosci. 27, 2596–2605.

Lambertsen, K.L., Clausen, B.H., Babcock, A.A., Gregersen, R., Fenger, C., Nielsen, H.H., Haugaard, L.S., Wirenfeldt, M., Nielsen, M., Dagnaes-Hansen, F., Bluethmann, H., Faergeman, N.J., Meldgaard, M., Deierborg, T., Finsen, B., 2009. Microglia protect neurons against ischemia by synthesis of tumor necrosis factor. J. Neurosci. 29, 1319–1330.

Lee, S.C., Liu, W., Brosnan, C.F., Dickson, D.W., 1994. GM-CSF promotes proliferation of human fetal and adult microglia in primary cultures. Glia 12, 309–318.

Liu, M.T., Keirstead, H.S., Lane, T.E., 2001. Neutralization of the chemokine CXCL10 reduces inflammatory cell invasion and demyelination and improves neurological function in a viral model of multiple sclerosis. J. Immunol. 167, 4091–4097.

Matsumura, M., Banba, N., Motohashi, S., Hattori, Y., 1999. Interleukin-6 and transforming growth factor-beta regulate the expression of monocyte chemoattractant protein-1 and colony-stimulating factors in human thyroid follicular cells. Life Sci. 65, PL129–PL135.

Matsuzaki, Y., Kinjo, K., Mulligan, R.C., Okano, H., 2004. Unexpectedly efficient homing capacity of purified murine hematopoietic stem cells. Immunity 20, 87–93.

McTigue, D.M., Popovich, P.G., Morgan, T.E., Stokes, B.T., 2000. Localization of transforming growth factor-beta1 and receptor mRNA after experimental spinal cord injury. Exp. Neurol. 163, 220–230.

Merkler, D., Metz, G.A., Raineteau, O., Dietz, V., Schwab, M.E., Fouad, K., 2001. Locomotor recovery in spinal cord-injured rats treated with an antibody neutralizing the myelin-associated neurite growth inhibitor Nogo-A. J. Neurosci. 21, 3665–3673.

Miao, T., Wu, D., Zhang, Y., Bo, X., Subang, M.C., Wang, P., Richardson, P.M., 2006. Suppressor of cytokine signaling-3 suppresses the ability of activated signal transducer and activator of transcription-3 to stimulate neurite growth in rat primary sensory neurons. J. Neurosci. 26, 9512–9519.

Mildenberger, M., Beach, T.G., McGeer, E.G., Ludgate, C.M., 1990. An animal model of prophylactic cranial irradiation: histologic effects at acute, early and delayed stages. Int. J. Radiat. Oncol. Biol. Phys. 18, 1051–1060.

Nesic, O., Xu, G.Y., McAdoo, D., High, K.W., Hulsebosch, C., Perez-Pol, R., 2001. IL-1 receptor antagonist prevents apoptosis and caspase-3 activation after spinal cord injury. J. Neurotrauma 18, 947–956.

Nishimoto, N., Sasai, M., Shima, Y., Nakagawa, M., Matsumoto, T., Shirai, T., Kishimoto, T., Yoshizaki, K., 2000. Improvement in Castleman's disease by humanized anti-interleukin-6 receptor antibody therapy. Blood 95, 56–61.

Okada, S., Nakamura, M., Mikami, Y., Shimazaki, T., Mihara, M., Ohsugi, Y., Iwamoto, Y., Yoshizaki, K., Kishimoto, T., Toyama, Y., Okano, H., 2004. Blockade of interleukin-6 receptor suppresses reactive astrogliosis and ameliorates functional recovery in experimental spinal cord injury. J. Neurosci. Res. 76, 265–276.

Okada, S., Nakamura, M., Katoh, H., Miyao, T., Shimazaki, T., Ishii, K., Yamane, J., Yoshimura, A., Iwamoto, Y., Toyama, Y., Okano, H., 2006. Conditional ablation of Stat3 or Socs3 discloses a dual role for reactive astrocytes after spinal cord injury. Nat. Med. 12, 829–834.

Okazaki, M., Yamada, Y., Nishimoto, N., Yoshizaki, K., Mihara, M., 2002. Characterization of anti-mouse interleukin-6 receptor antibody. Immunol. Lett. 84, 231–240.

Penkowa, M., Giralt, M., Lago, N., Camats, J., Carrasco, J., Hernandez, J., Molinero, A., Campbell, I.L., Hidalgo, J., 2003. Astrocyte-targeted expression of IL-6 protects the CNS against a focal brain injury. Exp. Neurol. 181, 130–148.

Ponomarev, E.D., Maresz, K., Tan, Y., Dittel, B.N., 2007. CNS-derived interleukin-4 is essential for the regulation of autoimmune inflammation and induces a state of alternative activation in microglial cells. J. Neurosci. 27, 10714–10721.

Popovich, P.G., Guan, Z., Wei, P., Huitinga, I., van Rooijen, N., Stokes, B.T., 1999. Depletion of hematogenous macrophages promotes partial hindlimb recovery and neuroanatomical repair after experimental spinal cord injury. Exp. Neurol. 158, 351–365.

Popovich, P.G., Guan, Z., McGaughy, V., Fisher, L., Hickey, W.F., Basso, D.M., 2002. The neuropathological and behavioral consequences of intraspinal microglial/macrophage activation. J. Neuropathol. Exp. Neurol. 61, 623–633.

Rapalino, O., Lazarov-Spiegler, O., Agranov, E., Velan, G.J., Yoles, E., Fraidakis, M., Solomon, A., Gepstein, R., Katz, A., Belkin, M., Hadani, M., Schwartz, M., 1998. Implantation of stimulated homologous macrophages results in partial recovery of paraplegic rats. Nat. Med. 4, 814–821.

Rinner, W.A., Bauer, J., Schmidts, M., Lassmann, H., Hickey, W.F., 1995. Resident microglia and hematogenous macrophages as phagocytes in adoptively transferred experimental autoimmune encephalomyelitis: an investigation using rat radiation bone marrow chimeras. Glia 14, 257–266.

Romano, M., Sironi, M., Toniatti, C., Polentarutti, N., Fruscella, P., Ghezzi, P., Faggioni, R., Luini, W., van Hinsbergh, V., Sozzani, S., Bussolino, F., Poli, V., Ciliberto, G., Mantovani, A., 1997. Role of IL-6 and its soluble receptor in induction of chemokines and leukocyte recruitment. Immunity 6, 315–325.

Rotshenker, S., Reichert, F., Gitik, M., Haklai, R., Elad-Sfadia, G., Kloog, Y., 2008. Galectin-3/MAC-2, Ras and PI3K activate complement receptor-3 and scavenger receptor-AI/II mediated myelin phagocytosis in microglia. Glia 56, 1607–1613.

Sato, K., Tsuchiya, M., Saldanha, J., Koishihara, Y., Ohsugi, Y., Kishimoto, T., Bendig, M.M., 1993. Reshaping a human antibody to inhibit the interleukin 6-dependent tumor cell growth. Cancer Res. 53, 851–856.

Saville, L.R., Pospisil, C.H., Mawhinney, L.A., Bao, F., Simedrea, F.C., Peters, A.A., O'Connell, P.J., Weaver, L.C., Dekaban, G.A., 2004. A monoclonal antibody to CD11d reduces the inflammatory infiltrate into the injured spinal cord: a potential neuroprotective treatment. J. Neuroimmunol. 156, 42–57.

Schilling, M., Besselmann, M., Muller, M., Strecker, J.K., Ringelstein, E.B., Kiefer, R., 2005. Predominant phagocytic activity of resident microglia over hematogenous macrophages following transient focal cerebral ischemia: an investigation using green fluorescent protein transgenic bone marrow chimeric mice. Exp. Neurol. 196, 290–297.

Schwartz, M., Lazarov-Spiegler, O., Rapalino, O., Agranov, I., Velan, G., Hadani, M., 1999. Potential repair of rat spinal cord injuries using stimulated homologous macrophages. Neurosurgery 44, 1041–1045 discussion 1045-1046.

Sedgwick, J.D., Schwender, S., Imrich, H., Dorries, R., Butcher, G.W., ter Meulen, V., 1991. Isolation and direct characterization of resident microglial cells from the normal and inflamed central nervous system. Proc. Natl. Acad. Sci. U. S. A. 88, 7438–7442.

Sharma, H.S., Winkler, T., Stalberg, E., Gordh, T., Alm, P., Westman, J., 2003. Topical application of TNF-alpha antiserum attenuates spinal cord trauma induced edema formation, microvascular permeability disturbances and cell injury in the rat. Acta Neurochir. Suppl. 86, 407–413.

Steinmetz, M.P., Horn, K.P., Tom, V.J., Miller, J.H., Busch, S.A., Nair, D., Silver, D.J., Silver, J., 2005. Chronic enhancement of the intrinsic growth capacity of sensory neurons combined with the degradation of inhibitory proteoglycans allows functional regeneration of sensory axons through the dorsal root entry zone in the mammalian spinal cord. J. Neurosci. 25, 8066–8076.

Swartz, K.R., Liu, F., Sewell, D., Schochet, T., Campbell, I., Sandor, M., Fabry, Z., 2001. Interleukin-6 promotes post-traumatic healing in the central nervous system. Brain Res. 896, 86–95.

Tamura, T., Udagawa, N., Takahashi, N., Miyaura, C., Tanaka, S., Yamada, Y., Koishihara, Y., Ohsugi, Y., Kumaki, K., Taga, T., et al., 1993. Soluble interleukin-6 receptor triggers osteoclast formation by interleukin 6. Proc. Natl. Acad. Sci. U. S. A. 90, 11924–11928.

Tuna, M., Polat, S., Erman, T., Ildan, F., Gocer, A.I., Tuna, N., Tamer, L., Kaya, M., Cetinalp, E., 2001. Effect of anti-rat interleukin-6 antibody after spinal cord injury in the rat: inducible nitric oxide synthase expression, sodium- and potassium-activated, magnesium-dependent adenosine-5′-triphosphatase and superoxide dismutase activation, and ultrastructural changes. J. Neurosurg. 95, 64–73.

Turrin, N.P., Plante, M.M., Lessard, M., Rivest, S., 2007. Irradiation does not compromise or exacerbate the innate immune response in the brains of mice that were transplanted with bone marrow stem cells. Stem Cells 25, 3165–3172.

Van Wagoner, N.J., Benveniste, E.N., 1999. Interleukin-6 expression and regulation in astrocytes. J. Neuroimmunol. 100, 124–139.

Therapeutic potential of appropriately evaluated safe-induced pluripotent stem cells for spinal cord injury

Osahiko Tsuji[a,b,1], Kyoko Miura[a,c,1], Yohei Okada[a,d], Kanehiro Fujiyoshi[a,b], Masahiko Mukaino[a,e], Narihito Nagoshi[a,b,f], Kazuya Kitamura[a,b], Gentaro Kumagai[a,g], Makoto Nishino[a], Shuta Tomisato[a], Hisanobu Higashi[a], Toshihiro Nagai[h], Hiroyuki Katoh[a,b,f], Kazuhisa Kohda[a], Yumi Matsuzaki[a], Michisuke Yuzaki[a], Eiji Ikeda[i,j], Yoshiaki Toyama[b], Masaya Nakamura[b,2], Shinya Yamanaka[c], and Hideyuki Okano[a,2]

Departments of [a]Physiology and [b]Orthopedic Surgery, School of Medicine, Keio University, Shinjuku, Tokyo 160-8582, Japan; [c]Center for Induced Pluripotent Stem Cell Research and Application, Kyoto University, Kyoto 606-8507, Japan; [d]Kanrinmaru-Project and Departments of [e]Rehabilitation Medicine, [h]Electron Microscope Laboratory, and [i]Pathology, School of Medicine, Keio University, Tokyo 160-8582, Japan; [f]Department of Orthopedic Surgery, National Hospital Organization, Murayama Medical Center, Tokyo 208-0011, Japan; [g]Department of Orthopedic Surgery, Graduate School of Medicine, Hirosaki University, Aomori 036-8560, Japan; and [j]Department of Pathology, Graduate School of Medicine, Yamaguchi University, Yamaguchi 755-8505, Japan

Edited by Fred Gage, Salk Institute, San Diego, CA, and approved June 3, 2010 (received for review September 3, 2009)

Various types of induced pluripotent stem (iPS) cells have been established by different methods, and each type exhibits different biological properties. Before iPS cell-based clinical applications can be initiated, detailed evaluations of the cells, including their differentiation potentials and tumorigenic activities in different contexts, should be investigated to establish their safety and effectiveness for cell transplantation therapies. Here we show the directed neural differentiation of murine iPS cells and examine their therapeutic potential in a mouse spinal cord injury (SCI) model. "Safe" iPS-derived neurospheres, which had been pre-evaluated as nontumorigenic by their transplantation into nonobese diabetic/severe combined immunodeficiency (NOD/SCID) mouse brain, produced electrophysiologically functional neurons, astrocytes, and oligodendrocytes in vitro. Furthermore, when the safe iPS-derived neurospheres were transplanted into the spinal cord 9 d after contusive injury, they differentiated into all three neural lineages without forming teratomas or other tumors. They also participated in remyelination and induced the axonal regrowth of host 5HT$^+$ serotonergic fibers, promoting locomotor function recovery. However, the transplantation of iPS-derived neurospheres pre-evaluated as "unsafe" showed robust teratoma formation and sudden locomotor functional loss after functional recovery in the SCI model. These findings suggest that pre-evaluated safe iPS clone-derived neural stem/progenitor cells may be a promising cell source for transplantation therapy for SCI.

neural stem/progenitor cell | cell transplantation | regenerative medicine | remyelination | axonal regrowth

Given their ability to generate all types of neural cells, neural stem/progenitor cells (NS/PCs) are a promising source for cell replacement therapy for various intractable CNS disorders (reviewed in refs. 1–6). Notably, ES cells have great developmental plasticity and can be induced to become NS/PCs with specific differentiation potentials (7–11), making them a major candidate for cell replacement therapies for CNS disorders (12–16). The clinical use of ES cells is complicated, however, by ethical and immunological concerns, both of which might be overcome by using pluripotent stem cells derived directly from a patient's own somatic cells (17).

We recently reported the establishment of induced pluripotent stem (iPS) cells from mouse fibroblasts by the retroviral introduction of four factors (*Oct3/4*, *Sox2*, *Klf4*, and *c-Myc*) with selection for *Fbxo15* expression (18) and *Nanog* expression (19, 20). Compared with *Fbxo15*-selected iPS cells, *Nanog*-selected iPS cells more closely resembled ES cells' gene-expression pattern and could contribute to germline-competent adult chimeras (19–21). More recently, we and others (22, 23) generated iPS cells without using *c-Myc* retroviruses, albeit with lower efficiency. The successful establishment of these iPS cell lines, along with initial reports showing efficacy in the therapeutic use of iPS cells in rodent models of sickle cell anemia (24) and Parkinson disease (25), led us to examine the use of iPS cells as a treatment for spinal cord injury (SCI).

A number of important issues need to be addressed before a clinical trial using iPS cells as a cell-therapy source for SCI is initiated. First, a detailed evaluation of iPS cells' potential to generate neural cells compared with ES cells is required. Second, iPS cells are likely to carry a higher risk of tumorigenicity than ES cells, due to the inappropriate reprogramming of these somatic cells, the activation of exogenous transcription factors, or other reasons (25–27). Thus, it is essential to confirm the safety of grafted iPS-derived NS/PCs. Finally, the effectiveness of iPS-derived NS/PC transplantation as a treatment for SCI must be evaluated.

In the previous study, we pre-evaluated iPS clones for safety by transplanting iPS-derived neurospheres into the NOD/SCID mouse brain (27). Here, we show that the transplantation of neurospheres derived from safe iPS cell clones into the injured spinal cord promoted functional recovery without any tumor formation. In contrast, the transplantation of neurospheres derived from unsafe iPS cells, showing robust teratoma formation in the NOD/SCID mouse brain, also resulted in initial functional recovery, but was later followed by teratoma formation and deterioration of locomotor function. These data suggest that the evaluation of in vitro differentiation and in vivo tumorigenicity are important for identifying safe iPS clones for cell therapy, and that the NS/PCs derived from iPS clones deemed safe by such pre-evaluation are a promising source for cell therapy for SCI.

Results

Pre-Evaluated Safe MEF-iPS Cells Exhibit ES-Like Neural Differentiation Potentials in Vitro. We previously reported the neural differentiation of 36 independent murine iPS cell clones (27). The results of this study led us to classify several iPS clones as safe or unsafe

Author contributions: O.T., K.M., M. Nakamura, S.Y., and H.O. designed research; O.T., K.M., Y.O., K.F., M.M., N.N., K. Kitamura, G.K., M. Nishino, S.T., H.H., T.N., H.K., E.I., and H.O. performed research; O.T. and K.M. contributed new reagents/analytic tools; O.T., K.M., Y.O., K.F., M.M., N.N., K. Kitamura, G.K., H.K., K. Kohda, Y.M., M.Y., E.I., Y.T., M. Nakamura, S.Y., and H.O. analyzed data; and O.T., K.M., Y.O., K.F., H.K., E.I., M. Nakamura, and H.O. wrote the paper.

The authors declare no conflict of interest.

This article is a PNAS Direct Submission.

[1]O.T. and K.M. contributed equally to this work.

[2]To whom correspondence may be addressed. E-mail: hidokano@sc.itc.keio.ac.jp or masa@sc.itc.keio.ac.jp.

This article contains supporting information online at www.pnas.org/lookup/suppl/doi:10.1073/pnas.0910106107/-/DCSupplemental.

clones, according to the teratoma-forming activity of the iPS-derived neurospheres after transplantation into the NOD/SCID mouse brain.

Here, we first performed a detailed examination of the neural differentiation potential of a safe iPS clone, 38C2, which was established from mouse embryonic fibroblasts (MEFs) by the introduction of four factors, including *c-Myc*, and by the selection for *Nanog* expression (19, 28), and compared them with mouse ES cells (EB3) (29, 30). 38C2 iPS cells and EB3 ES cells were induced into embryoid bodies (EBs) in medium containing a low concentration of retinoic acid, then dissociated and cultured in suspension in serum-free medium with FGF-2 for 7 or 8 d to form primary neurospheres (PNS) (38C2 iPS/EB3 ES-PNS) (29). These PNSs were dissociated and formed secondary neurospheres (38C2 iPS/EB3 ES-SNS) under the same conditions (Fig. 1*A*). To induce further differentiation, 38C2 iPS-SNSs were adherently cultured in the absence of FGF-2, resulting in the generation of Tuj1$^+$ neurons (4.9 ± 0.8%), GFAP$^+$ astrocytes (11.3 ± 1.2%), and CNPase$^+$ oligodendrocytes (3.7 ± 0.9%), as well as Nestin$^+$ neural progenitor cells (25.9 ± 6.5%; Fig. 1 *B* and *C*), suggesting that 38C2 iPS-SNS have similar differentiation potentials to EB3 ES-SNS. The 38C2 iPS-PNSs could also generate TH$^+$ catecholaminergic, 5HT$^+$ serotonergic, and GAD67$^+$ GABAergic neurons (Fig. S1). RT-PCR analysis of the expression of cell-type-specific markers in the progeny of the 38C2 iPS cells showed drastic decrease of the expression of undifferentiated ES cell marker genes, such as *Nanog*, *Eras*, and *Oct3/4*, and the up-regulation of neural markers such as *Sox1*, *βIII-tubulin,* and *GFAP* during the neural differentiation of 38C2 iPS cells, similar to EB3 ES cells (Fig. 1*D*).

Moreover, electrophysiological analysis using whole-cell patch clamping in both the 38C2 iPS-PNS– and EB ES-PNS–derived neurons after 21–28 d of adherent differentiation showed tetrodotoxin (TTX; 1 μM)-sensitive repetitive action potentials in the current-clamp mode [38C2 iPS-PNS (n = 11 of 16) and EB3 ES-PNS (n = 5 of 7)] (Fig. S2*A*) and very rapid inward currents immediately followed by transient outward currents in voltage-clamp mode (Fig. S2*B* 1 and 2). Steady outward currents, similar to those mediated by delayed-rectifier K$^+$ channels, were also observed (Fig. S2 *B*1 and *D*). These findings suggest that 38C2 iPS-PNSs produced neuronal cells equipped with functional channels that could generate and modify action potentials (*SI Text*).

Safe MEF-iPS Cells Can Differentiate into Trilineage Neural Cells in the Injured Spinal Cord Without Tumorigenesis. Previously, we confirmed that SNSs from the safe 38C2 MEF-iPS cell clone survived and showed no teratoma-forming activity in the NOD/SCID mouse brain for 24 wk after transplantation (27) (Fig. S3). 38C2 iPS-SNSs that were transplanted into the intact spinal cord survived and differentiated into trilineage neural cells without any tumorigenesis (Fig. S4). Next, to evaluate their therapeutic effects in the mouse SCI model, we transplanted 38C2 iPS-SNSs into the contused spinal cord 9 d after injury and compared them with EB3 ES-SNSs, using adult fibroblasts and PBS as controls. We also made a comparison with 38C2 iPS-PNSs, because we recently confirmed that the transplantation of ES cell-derived SNSs, but not PNSs, provides therapeutic benefit after SCI (31). We transplanted 38C2 iPS-SNSs that had been prelabeled by lentivirus to express both CBR*luc* and mRFP (32, 33) into the lesion epicenter 9 d after the injury. Bioluminescence imaging (BLI) analysis (34), which detects luciferase photon signals only from living cells, revealed an approximate graft survival rate of 18% at 35 d after transplantation (Fig. 2*A*). We also histologically confirmed that the grafted cells survived and exhibited no apparent evidence of tumorigenesis (Fig. 2*B*), and that there were no Nanog$^+$ cells (Fig. S5), at least during our observation

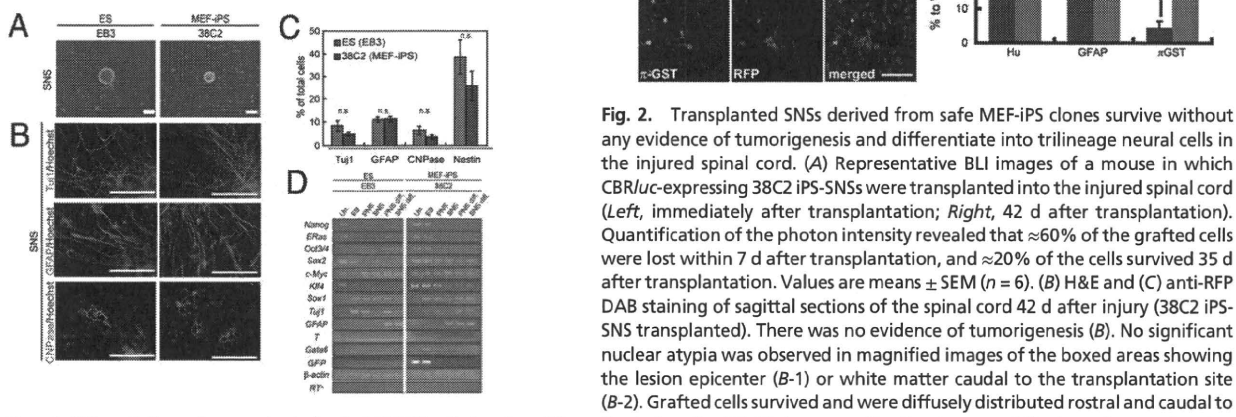

Fig. 2. Transplanted SNSs derived from safe MEF-iPS clones survive without any evidence of tumorigenesis and differentiate into trilineage neural cells in the injured spinal cord. (*A*) Representative BLI images of a mouse in which CBR*luc*-expressing 38C2 iPS-SNSs were transplanted into the injured spinal cord (*Left*, immediately after transplantation; *Right*, 42 d after transplantation). Quantification of the photon intensity revealed that ≈60% of the grafted cells were lost within 7 d after transplantation, and ≈20% of the cells survived 35 d after transplantation. Values are means ± SEM (n = 6). (*B*) H&E and (*C*) anti-RFP DAB staining of sagittal sections of the spinal cord 42 d after injury (38C2 iPS-SNS transplanted). There was no evidence of tumorigenesis (*B*). No significant nuclear atypia was observed in magnified images of the boxed areas showing the lesion epicenter (*B*-1) or white matter caudal to the transplantation site (*B*-2). Grafted cells survived and were diffusely distributed rostral and caudal to the lesion site (*C*). Higher-magnification images of the boxed areas showing the lesion site (C-1) and white matter caudal to the lesion site (C-2). *Lesion epicenter. (*D*) Immunohistochemical analyses of 38C2 iPS-SNSs grafted into spinal cord 42 d after injury, revealing grafted cells double-positive for RFP and markers of neural lineages. (*E*) Quantitative analyses of Hu$^+$ neurons, GFAP$^+$ astrocytes, and π-GST$^+$ oligodendrocytes. Values are means ± SEM (n = 3 each; *P < 0.05, **P < 0.01).

Fig. 1. Neural differentiation of pre-evaluated safe MEF-iPS cells in vitro. (*A*) Neurospheres derived from EB3 ES cells and 38C2 iPS cells. (Scale bar: 200 μm.) (*B*) Immunocytochemical analysis of neural cell marker proteins in the differentiated SNSs derived from EB3 ES and 38C2 iPS cells. (Scale bar: 100 μm.) (*C*) Neural differentiation efficiencies of neurospheres derived from EB3 ES and 38C2 iPS cells. (n = 5, n.s.). (*D*) RT-PCR analysis of undifferentiated cells (Un.), EBs, PNSs, SNSs, differentiated PNSs (PNS diff.), and SNSs (SNS diff.) of the EB3-ES and 38C2 iPS cells.